

Chapter 2

The hyperfine shift

Contents

2.1. The hyperfine shift	29
2.2. The magnetic nucleus–unpaired electron interaction	31
2.2.1. The Fermi contact coupling	32
2.2.2. The dipolar coupling	35
2.2.2.1. Metal-centered point-dipole approximation	35
2.2.2.2. Ligand-centered contributions	41
2.3. Shift and spin patterns for protons and deuterons in solution	41
2.4. Proton hyperfine coupling and conformation	53
2.5. The origin of the shifts in heteronuclei	57
2.6. When is metal centered pseudocontact shift expected	61
2.7. Attempts to factorize contact and pseudocontact shifts	63
2.8. The case of lanthanides and actinides	65
2.8.1. Electronic properties of lanthanides	65
2.8.2. The pseudocontact contribution to the hyperfine shifts	66
2.8.3. The contact contribution to the hyperfine shifts	67
2.8.4. Separation of pseudocontact and contact contributions	68
2.8.5. Lanthanides as pseudocontact shift reagents	70
2.9. The pseudocontact shifts in paramagnetic metalloproteins	71
References	72

2.1. The hyperfine shift

How does the nucleus sense the electron? As mentioned in Section 1.7.4, nuclear and electron spins continuously change their levels but the population distribution remains constant at a given temperature. The change of level occurs through mechanisms which are different or have different degrees of efficiency for the two sets of spins, with the result that electrons relax orders of magnitude faster than nuclei. As a consequence, the nucleus in each of its M_I energy levels sees one electron rapidly changing its orientation among the M_S levels. The nucleus therefore senses an average magnetic moment of the electron which would be zero if the populations of the M_S levels were equal. As it is not so, the nucleus senses the average magnetic moment $\langle \mu \rangle$ which is just proportional to $\langle S_z \rangle$ (see Section 1.6). It should be recalled that $\langle S_z \rangle$ is negative (Eq. (1.31)) due to the slight excess of population in the $M_S = -\frac{1}{2}$ state.

The unpaired electron has the further complication that it is not localized on a single point but, in general, is delocalized on the entire molecule. So, in every point of space where the molecular orbital (MO) containing the unpaired electron has a non-zero value, the average electron magnetic moment sensed by the nucleus is different from zero and is proportional to $\langle S_z \rangle$ times the so-called spin density ρ , which for a half-filled orbital is simply given by the square of the wavefunction at that point.

The situation is still further complicated by the fact that the presence of an unpaired electron in an MO polarizes the paired electrons in the core. This is called spin polarization. The MO containing the paired electrons is modified by the presence of the unpaired electron in another MO in such a way that the electron with the spin aligned with the unpaired electron will have a slight preference to occupy the region of space of its MO which is closer to the unpaired electron itself (this is a manifestation of Hund's rule). Conversely, the other electron with spin antiparallel to the unpaired electron will have a slight preference to occupy regions of its MO far from the unpaired electron. This is illustrated in Fig. 2.1 for the case of atomic orbitals.

At this point we recall that the unpaired electron may have some probability to sit just on the nucleus. Type s orbitals have maximal electron density on the nucleus, as their wavefunction is of the type $\exp(-r)$, where r is the electron–nucleus distance. Therefore, if the unpaired electron occupies an s orbital, or an MO containing an s orbital, there will be a finite probability that the electron resides on that nucleus. The amount of unpaired electrons residing on the nucleus is the spin density ρ at the nucleus. The spin density at the nucleus or in any other point is, in general, not

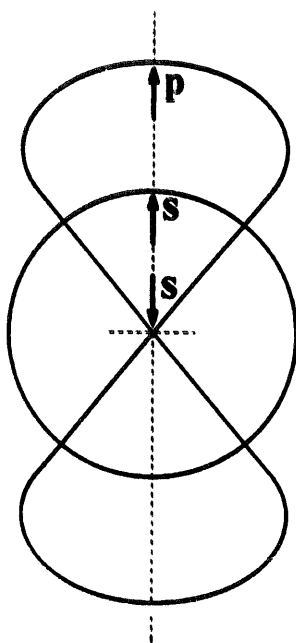


Fig. 2.1. The unpaired electron in a p orbital affects the distribution of the two paired electrons in a 1s orbital.

just the positive quantity arising from the direct delocalization explained above, but also contains contributions due to spin polarization of paired electrons. The latter mechanism accounts for the presence of spin density on nuclei when the unpaired electron occupies p or d orbitals, which have a node at the nucleus (Fig. 2.2). However, the unpaired electron on a p (or d) orbital can spin-polarize the electron pair occupying any s orbital. For instance, the electron of a 1s pair with the same spin as the unpaired electron in a p or d orbital will preferentially be in the outer part of the 1s orbital, whereas the electron with reverse spin will preferentially be in the inner part of the 1s orbital (Fig. 2.1). The two electrons of the pair will now have different probabilities to be at the nucleus. The difference provides a contribution of that orbital to the spin density at the nucleus. This contribution has opposite sign with respect to the contribution from the spin density in the orbital containing the unpaired electron. Since the unpaired electron has excess spin value $M_S = -\frac{1}{2}$ (*positive spin density*), the spin density at the nucleus arises from slight excess spin value $M_S = \frac{1}{2}$, and is thus negative. Note, therefore, that although the unpaired electron always preferentially aligns with its spin along the external magnetic field, spin polarization may induce on the nucleus negative spin density as if the electron were polarized opposite to the magnetic field.

2.2. The magnetic nucleus–unpaired electron interaction

In principle the magnetic nucleus senses a magnetic moment of the electron on itself and all over the space. We have seen that such magnetic moment is the result of both direct delocalization of unpaired electrons and spin polarization. The problem of the nucleus–electron interaction is therefore very complex. As mentioned earlier,

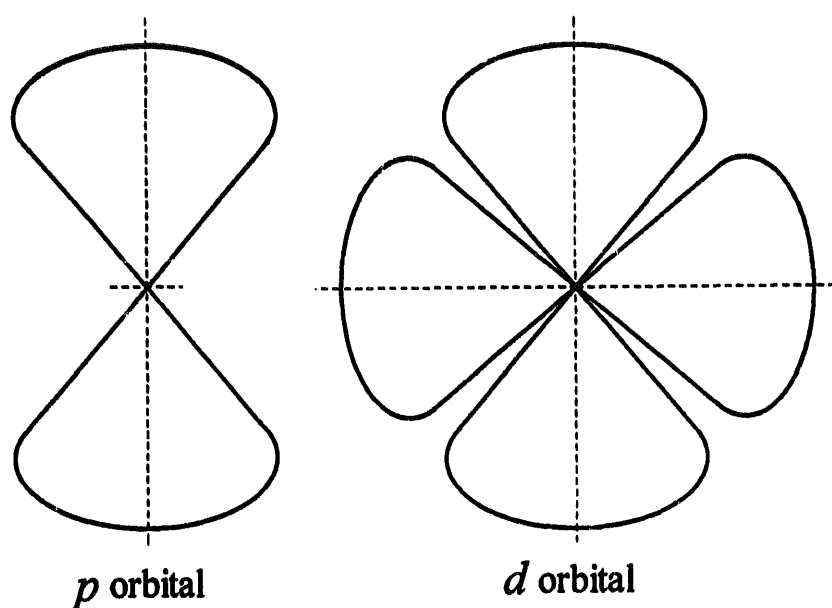


Fig. 2.2. p and d orbitals showing that the electron density at the nucleus is zero.

this is the hyperfine interaction. It is convenient to separately consider the spin density on the nucleus itself and then the spin density outside it. The former part of the interaction is called contact or Fermi contact interaction. The latter is called dipolar interaction because it is a through space interaction which can be described by the dipolar interaction of two magnetic dipoles. Of course, the evaluation of the dipolar interaction requires, in principle, the evaluation of the integral all over the space of the interaction energy between the resonating nucleus and the spin density on each point of the space.

2.2.1. The Fermi contact coupling

The contact shift is given by an additional magnetic field generated at the nucleus by the electron magnetic moment located at the nucleus itself. The latter magnetic moment originates from the spin density at the nucleus, weighted by $\langle S_z \rangle$. For an isolated paramagnet $\langle S_z \rangle$ is always negative. In contrast, spin density can be either positive or negative. Therefore, if the excess spin value is $-\frac{1}{2}$, the contribution to the magnetic field will be positive (Fig. 2.3) and the chemical shift in frequency will be positive. The reverse holds for $+\frac{1}{2}$ spin. We recall again that unpaired electrons do have excess $-\frac{1}{2}$ spin but, mainly due to spin polarization, excess $+\frac{1}{2}$ spin can be present on a given nucleus. The chemical shift will also depend on the amount of spin density at the nucleus. For each s orbital the spin density ρ is given by

$$\rho = \Psi_{-1/2}(0)^2 - \Psi_{1/2}(0)^2 \quad (2.1)$$

where $\Psi(0)$ is the value of the MO wavefunction at zero distance from the nucleus for $-\frac{1}{2}$ and $\frac{1}{2}$ spins. The spin density (when normalized to one electron) is proportional to what is called the contact coupling constant A , which expresses how much the nucleus and the electron sense each other:

$$A = \frac{\mu_0}{3S} h \gamma_I g_e \mu_B \sum_i \rho_i \quad (2.2)$$

where the sum is over all the s orbitals of the nucleus. Since the s orbitals do not have orbital magnetic moment, $g = g_e = 2.0023$. A is an energy, which in SI units is expressed in joule. Sometimes it is convenient to have it in hertz or in radians per second, and then we have to divide A by h or by \hbar ($\hbar = h/2\pi$). In magnetic resonance there often is a factor 2π which complicates life. The frequency which we refer to is the angular frequency or the Larmor precession frequency. Such frequency ω is such that $\omega = 2\pi\nu$ (Eq. (1.41)), where ν is the frequency in hertz. Therefore, ω is expressed in radians per second. The energy is

$$E = h\nu = \hbar \frac{\omega}{2\pi} = \hbar\omega \quad (2.3)$$

In order to express the energy in wavenumbers, we should remember that $E = hc/\lambda$, and then E is proportional to the inverse of a length.

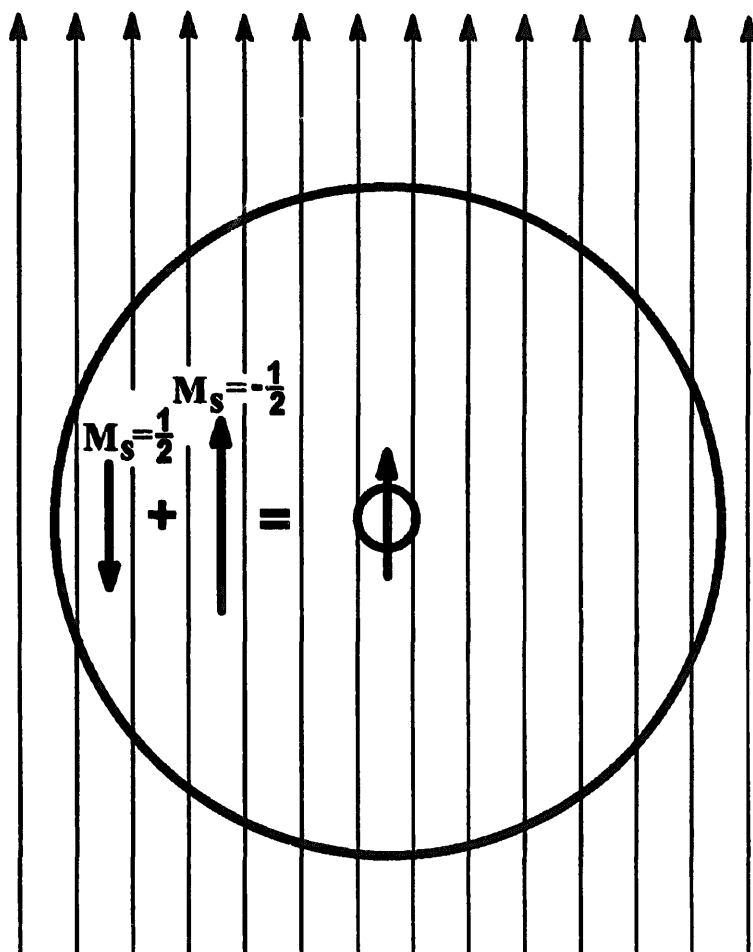


Fig. 2.3. Excess $-\frac{1}{2}$ electron spin density contributes a magnetic field at the nucleus that adds to the external magnetic field.

In quantum mechanical terms, the Hamiltonian for the contact interaction is

$$\mathcal{H} = A \mathbf{I} \cdot \mathbf{S} \quad (2.4)$$

and the energy is obtained by evaluating the matrix elements $\langle \Psi_{S, M_S, I, M_I} | \mathcal{H} | \Psi_{S, M_S, I, M_I} \rangle$. In the high field approximation ($g_e \mu_B B_0 \gg A$) the contact contribution to the chemical shift is (Appendix II) [1]

$$\delta^{\text{con}} = \frac{A}{h} \frac{g_e \mu_B S(S+1)}{3\gamma_I kT} \quad (2.5)$$

The nuclear I value of the resonating nucleus does not appear in Eq. (2.5) because the frequency is referred to any $\Delta M_I = 1$ transition. By using the definition of $\langle S_z \rangle$ of Eq. (1.31), the following relation is obtained (Appendix II):

$$\delta^{\text{con}} = -\frac{A}{h\gamma_I B_0} \langle S_z \rangle \quad (2.6)$$

Eq. (2.6) tells us that the fractional increase in frequency is due to the presence of unpaired spin density. No nuclear parameter is contained in the expression of the contact shift. The γ_I appearing in both Eqs. (2.5) and (2.6) cancel the γ_I contained in A (Eq. (2.2)). If we remember that $\langle S_z \rangle$ is negative for a free electron in a magnetic field (excess population of the $-\frac{1}{2}$ state), then the shift is positive.

We should note that if $g = g_e$, the contact shift is isotropic (independent of orientation). If g is different from g_e and anisotropic (see Section 1.4), then the contact shift is also anisotropic. The anisotropy of the shift is due to the fact that the energy spreading of the Zeeman levels is different for each orientation (see Fig. 1.16) and therefore the value of $\langle S_z \rangle$ will be orientation dependent. On the contrary, the contact coupling is a constant whose value does not depend on the molecular orientation. Therefore, A in Eq. (2.4) is different from A in Eq. (1.51).

Let us suppose now that we have a solid with all molecules aligned with one another (Fig. 2.4) and that we perform the NMR experiment on a single crystal. If g of the S manifold equals g_e , the contact shift contribution will be independent of the crystal orientation in the magnetic field. If, however, g has a different value in any kk direction (see Eq. (1.21)), then the contact shift will be orientation dependent. In fact, the expectation value of S_z depends on the energy separation of the M_S levels and then on the actual g_{kk} value. The value of $\langle S_z \rangle$ represents a dimensionless proportionality constant which reduces the interaction energy between a nucleus and a full unpaired electron.

$$\delta_{kk}^{\text{con}} = \frac{A}{h} \frac{g_{kk} \mu_B S(S+1)}{3\gamma_I kT} \quad (2.7)$$

Experimental evidence for this behavior will be given in Chapter 8. When the solid is dissolved in a liquid, the rotational rate of the molecules is fast with respect to the difference in hyperfine shift due to the electron Zeeman anisotropy, and the

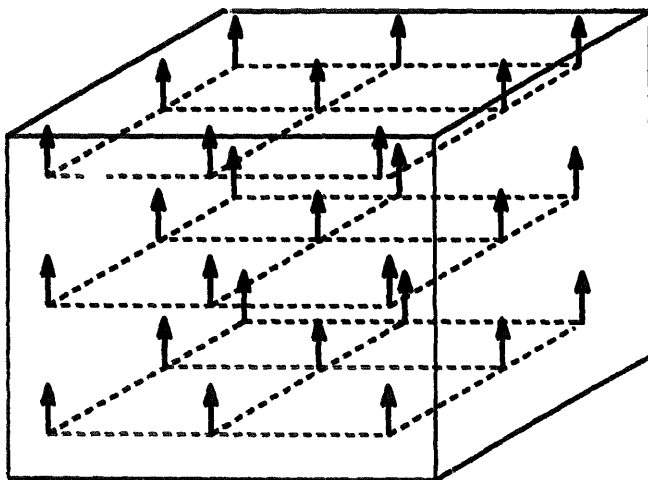


Fig. 2.4. Ideal crystal with all molecules iso-oriented.

contact shift will be an average:

$$\delta_{\text{sol}}^{\text{con}} = \frac{A}{\hbar} \frac{\bar{g}\mu_B S(S+1)}{3\gamma_I kT} \quad (2.8)$$

Typical values for proton hyperfine shift anisotropy are hardly larger than 10^5 s^{-1} , i.e. much smaller than τ_r^{-1} for all practical cases. Note that the g value contained in A (Eq. (2.2)) is still g_e because the s electron has no orbital magnetic moment.

A more correct form, which includes ZFS and the modification of the orbital wavefunctions upon application of the external magnetic field, is

$$\delta_{\text{sol}}^{\text{con}} = \frac{1}{\mu_0} \frac{A}{\hbar} \frac{1}{3\gamma_I \mu_B} \left(\frac{\chi_{xx}}{g_{xx}} + \frac{\chi_{yy}}{g_{yy}} + \frac{\chi_{zz}}{g_{zz}} \right) \quad (2.9)$$

where χ_{ii} and g_{ii} are the principal components of the molecular susceptibility (χ_M/N_A , cf. Eq. (1.27)), and g tensors. The reader can find a justification of it by comparing Eq. (2.9) with Eq. (2.8) through Eq. (1.38).

Note that all of these equations hold “rigorously” for $S = \frac{1}{2}$ systems with no orbital degeneracy in the ground state. For $S > \frac{1}{2}$ the equations hold as long as there is no ZFS. Under the above conditions, the contact shift has a $1/T$ dependence. In the presence of ZFS the use of Eqs. (2.5)–(2.8) becomes approximate and only Eq. (2.9) should in principle be used.

When different S manifolds are populated at the temperature of the experiment, due for example to low symmetry effects on near tetrahedral nickel(II) or near octahedral cobalt(II) complexes (see Section 2.6), every S manifold has its own hyperfine coupling, and the sum over the populated levels, each with its own hyperfine constant, should be used to calculate the shifts, with equations analogous to those derived in Chapter 5. This aspect is too often neglected in the literature, but once mention is made of the possible approximations, there is no alternative to the use of Eq. (2.8). Indeed, except in special cases [2,3], neither the g values nor the hyperfine coupling constants of each level, nor their energy separations are known.

2.2.2. The dipolar coupling

This contribution to the shift is quite difficult to evaluate, because in general the spin density distribution all over the space is not known. The approach to this problem should be stepwise. We first consider that the unpaired electron is localized on the metal nucleus in a paramagnetic metal complex. We refer to this as to the metal-centered point-dipole–point-dipole approximation. Surely this contribution will always be present and sometimes dominant. Then we will discuss the consequences of relaxing this condition. Even in the metal-centered approximation several cases should be discussed.

2.2.2.1. Metal-centered point-dipole approximation

Let us now refer to a set of molecules with their x , y and z axes iso-oriented in an idealized solid state (Fig. 2.5). If the external magnetic field is aligned with the

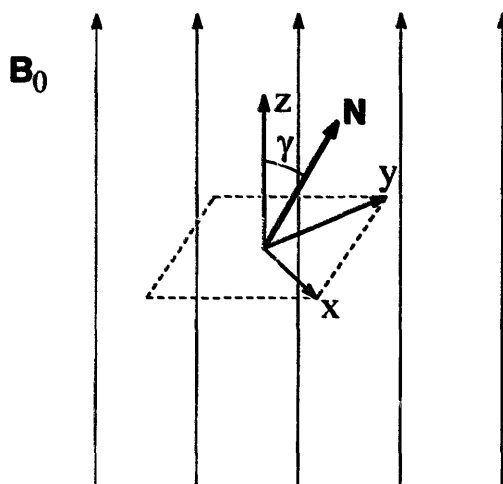


Fig. 2.5. A molecule possessing magnetic anisotropy, with the z axis oriented along the external magnetic field and a nucleus having a metal-nucleus vector at an angle γ with the external magnetic field.

z axis, the dipolar interaction energy between the nuclear magnetic moment and the electron magnetic moments, according to Eq. (1.4), is

$$E^{\text{dip}} = -\frac{\mu_0}{4\pi} h\gamma_I I_z \langle \mu \rangle \frac{1}{r^3} (3 \cos^2 \gamma - 1) \quad (2.10)$$

From Eqs. (1.27), (1.33) and (1.34) we can write E^{dip} in terms of the z component of the molecular susceptibility tensor $\chi = \chi_M/N_A$.

$$E^{\text{dip}} = -\frac{B_0}{4\pi r^3} h\gamma_I I_z \chi_{zz} (3 \cos^2 \gamma - 1) \quad (2.11)$$

where γ is the angle between the metal nucleus vector and the external magnetic field, which is coincident with the molecular χ_{zz} direction. In a generic kk direction, reference will be made to Fig. 2.6 and the energy, for an axial χ tensor, will be given by (Appendix III)

$$E^{\text{dip}} = -\frac{B_0}{4\pi r^3} h\gamma_I I_z [\chi_{\parallel} \cos^2 \alpha (3 \cos^2 \theta - 1) + \chi_{\perp} \sin^2 \alpha (3 \sin^2 \theta \cos^2 \Omega - 1) + \frac{3}{4}(\chi_{\parallel} + \chi_{\perp}) \sin 2\alpha \sin 2\theta \cos \Omega] \quad (2.12)$$

where α is the angle between the molecular z axis and the external magnetic field, θ is the angle between the metal-nucleus vector r and the molecular z axis, and Ω is an angle related to the projection of r on the molecular xy plane. Ω is zero when r lies in the plane defined by the external magnetic field and the molecular z axis.

From the dipolar interaction energy, the dipolar shift can be obtained by evaluating from Eq. (2.12) ΔE^{dip} between two states differing by $\Delta M_I = \pm 1$ and dividing it by

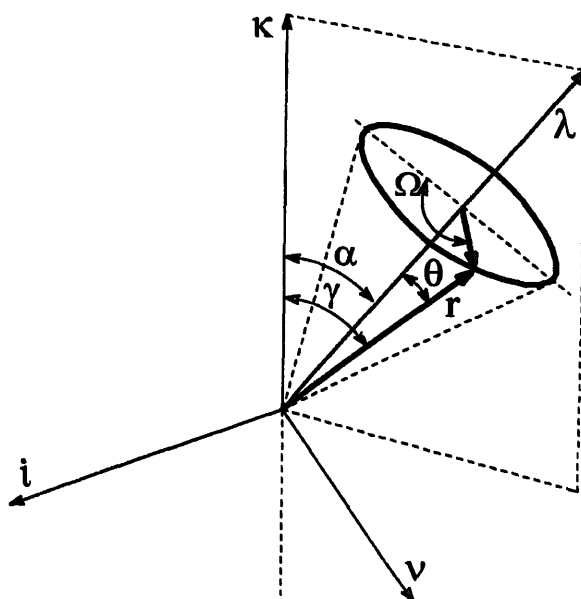


Fig. 2.6. A molecule possessing magnetic anisotropy, with the z axis oriented along a generic λ direction. α is the angle of the z axis with the external field direction κ ; θ is the angle between the metal-nucleus vector r and the z axis; γ is the angle between the metal-nucleus vector and the external field; Ω defines the position of r on the surface of the cone about λ .

the nuclear Zeeman energy $h\gamma_I B_0$ (Appendix III):

$$\delta^{\text{dip}} = \frac{1}{4\pi r^3} [\chi_{\parallel} \cos^2 \alpha (3 \cos^2 \theta - 1) + \chi_{\perp} \sin^2 \alpha (3 \sin^2 \theta \cos^2 \Omega - 1) + \frac{3}{4}(\chi_{\parallel} + \chi_{\perp}) \sin 2\alpha \sin 2\theta \cos \Omega] \quad (2.13)$$

This is indeed what is expected in ^1H ENDOR spectroscopy in single crystals. By integration of Eq. (2.13) over all molecular orientations, the following equation is obtained (Appendix III):

$$\delta^{\text{pc}} = \frac{1}{12\pi r^3} (\chi_{\parallel} - \chi_{\perp}) (3 \cos^2 \theta - 1) \quad (2.14)$$

This contribution to the shift is isotropic because it is already averaged out over all the orientations. Then it is similar to the contact shift and therefore it is called the pseudocontact shift δ^{pc} . In the literature it is also referred to as dipolar shift or isotropic dipolar shift.

Note that, when χ is isotropic, the pseudocontact shift is zero (Eq. (2.14)). This means that, when χ is isotropic, a dipolar shift is observed only in the solid state (Eq. (2.13) and Eq. (9) of Appendix III). That the dipolar interaction energy averages zero for isotropic χ can be easily verified by averaging Eq. (2.11) over all orientations, as

$$\int_{-1}^1 (3 \cos^2 \gamma - 1) d \cos \gamma = 0 \quad (2.15)$$

There is also an intuitive mode to see the effect of an isotropic electron magnetic moment on a nucleus. Fig. 2.7 illustrates that, indeed, the dipolar magnetic field experienced by the nucleus for different orientations of the metal-nucleus vector with the magnetic field changes sign, being positive when the vector is along the field and negative when the vector is perpendicular to the field. Therefore, one can accept that the average over all the orientations is zero. However, if the induced magnetic field changes intensity with the molecular orientation because χ is anisotropic, complete cancellation upon rotation does not occur any longer. It should be remembered that the anisotropy of χ (see Section 1.4) is due to orbital contributions to the magnetic moments.

The angular dependence of the pseudocontact shift is shown in Fig. 2.8. For $\theta = 54.74^\circ$, the pseudocontact shift is zero. If $\chi_{\parallel} > \chi_{\perp}$, then the pseudocontact shift is positive for θ values less than 54.74° . In the case in which χ_{xx} and χ_{yy} differ, then the angle Ω between the projection of the metal-nucleus vector on the xy plane and the y axis should also be considered (Fig. 2.9). The result is [4]

$$\delta^{\text{pc}} = \frac{1}{24\pi} \frac{1}{r^3} \{ [2\chi_{zz} - (\chi_{xx} + \chi_{yy})](3 \cos^2 \theta - 1) + 3(\chi_{xx} - \chi_{yy}) \sin^2 \theta \cos 2\Omega \} \quad (2.16)$$

The contribution of the in-plane anisotropy of χ varies with $\cos 2\Omega$.

Eq. (2.16), or its simplified version in the axial case, Eq. (2.14), are of general validity. However, the principal directions and components of the molecular χ tensor are seldom available. Pseudocontact shifts can be still evaluated by expressing the principal molecular magnetic susceptibility values as a function of the principal g values, in analogy with Eq. (1.38):

$$\chi_{kk} = \mu_0 \mu_B^2 g_{kk}^2 \frac{S(S+1)}{3kT} \quad (2.17)$$

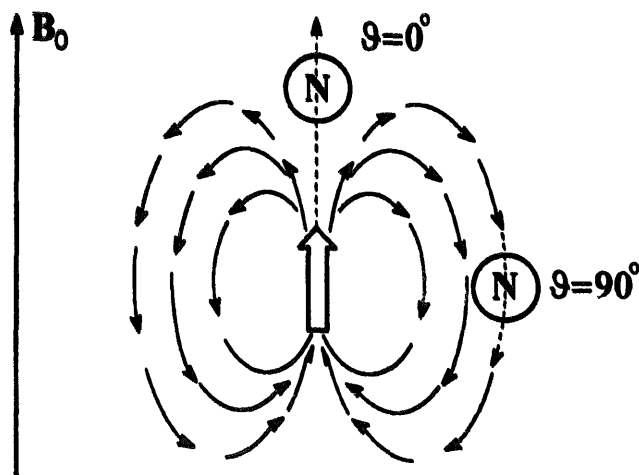


Fig. 2.7. A nucleus N immersed in the dipolar magnetic field of an electron spin, the latter aligned along the external magnetic field, experiences an extra field that adds ($\theta = 0^\circ$) or subtracts ($\theta = 90^\circ$) to the external field.

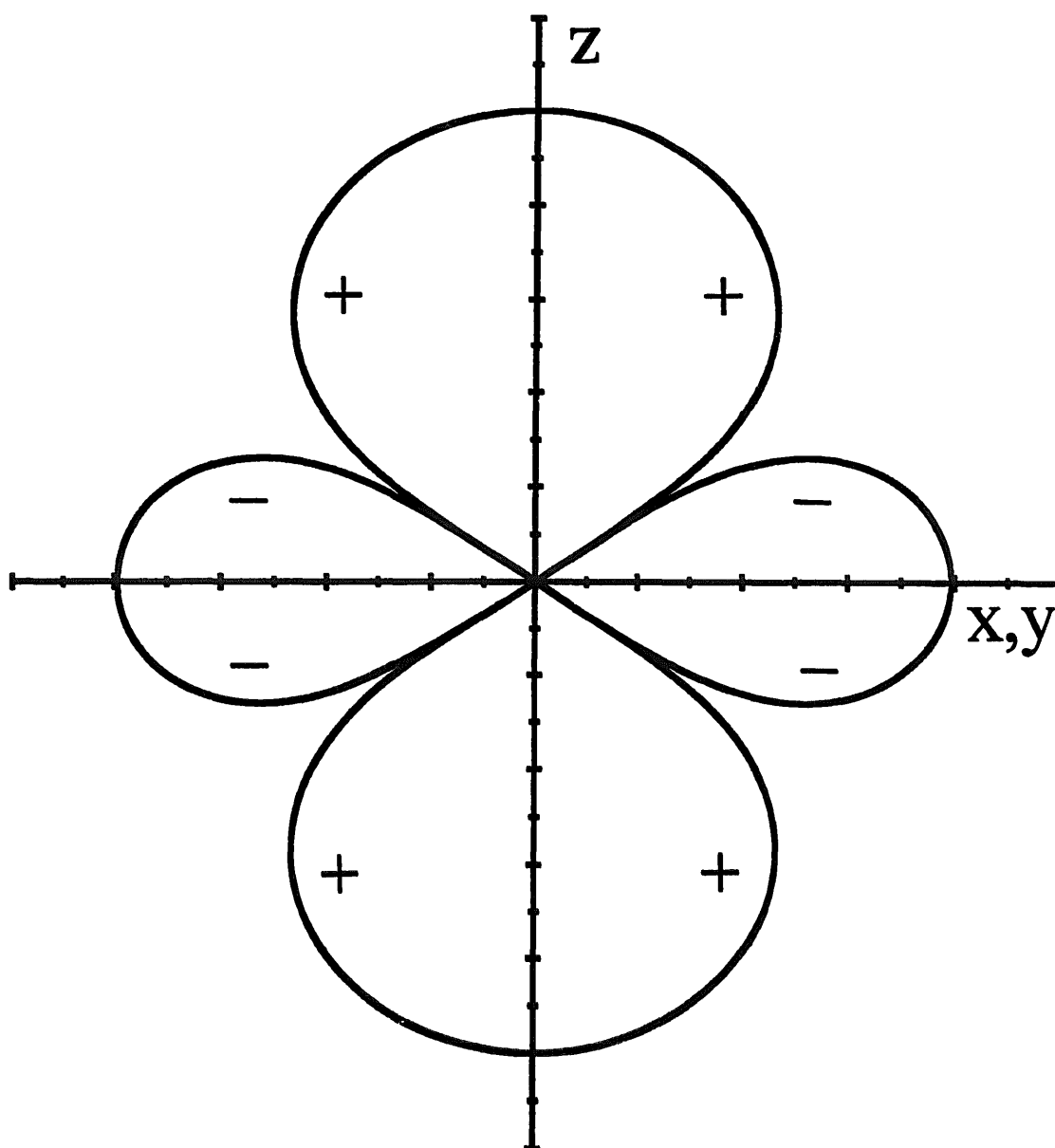


Fig. 2.8. Angular dependence of the pseudocontact shift for an axial system, shown as a surface of constant absolute value of δ^{pc} . In the example δ^{pc} is positive along the z axis and negative in the xy plane. The three-dimensional shape of the surface is similar to the representation of a d_{z^2} orbital.

As seen in Section 1.6, this approximation holds when the spin multiplet ground state is well isolated from excited electronic states, and ZFS is negligible. If $S = \frac{1}{2}$, the g values can easily be measured through EPR spectroscopy and the g directions can be determined by single-crystal EPR measurements. When the latter measurements are not available, sometimes the principal g directions can be guessed from the symmetry of the molecule, and an independent estimate of the pseudocontact shift can still be attempted.

By substituting the molecular χ values with the expression in Eq. (2.17), Eq. (2.14)

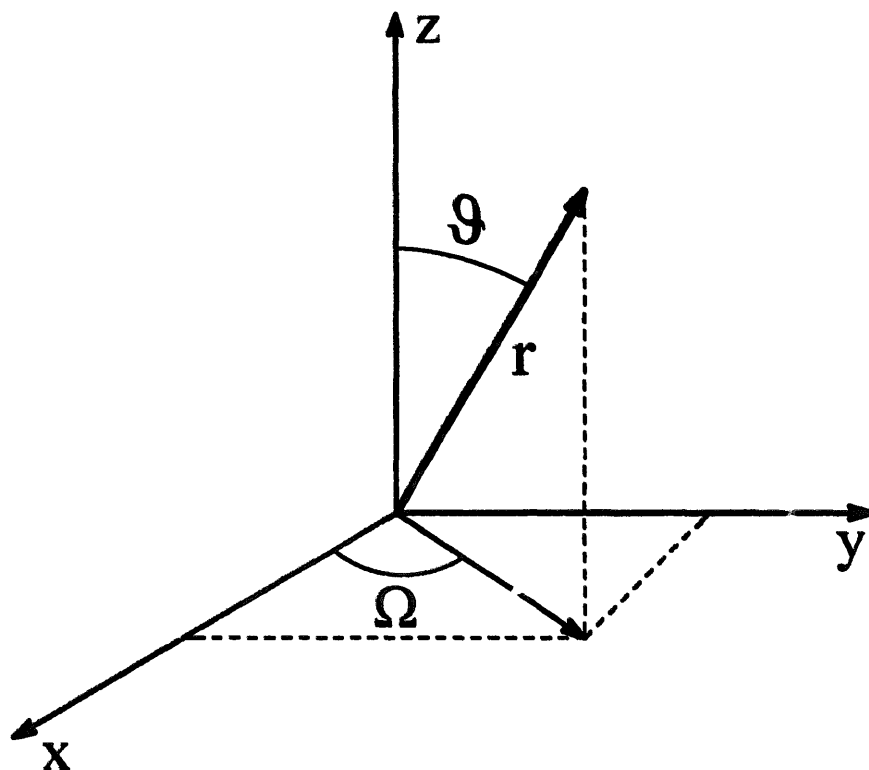


Fig. 2.9. Definition of the in-plane angle Ω for non-axial systems.

and (2.16) respectively become

$$\delta^{\text{pc}} = \frac{\mu_0}{4\pi} \frac{\mu_B^2 S(S+1)}{9kT} (g_{\parallel}^2 - g_{\perp}^2) \frac{1}{r^3} (3 \cos^2 \theta - 1) \quad (2.18)$$

$$\begin{aligned} \delta^{\text{pc}} = & \frac{\mu_0}{4\pi} \frac{\mu_B^2 S(S+1)}{18kT} \frac{1}{r^3} \{ [2g_{zz}^2 - (g_{xx}^2 + g_{yy}^2)] (3 \cos^2 \theta - 1) \\ & + 3(g_{xx}^2 - g_{yy}^2) \sin^2 \theta \cos 2\Omega \} \end{aligned} \quad (2.19)$$

As in the case of contact shift, the pseudocontact shift does not contain parameters of the resonating nucleus. At variance with contact shifts, the pseudocontact shifts can be evaluated even if more than one S multiplet is populated, provided that $\Delta\chi$ values are experimentally available. In the case of the contact shift, each S multiplet will have a different hyperfine coupling constant.

Note that Eqs. (2.18) and (2.19) (and, likewise, Eqs. (2.14) and (2.16)) can be written in a way analogous to Eq. (2.8):

$$\delta^{\text{pc}} = \frac{A^{\text{pc}}}{h} \frac{\bar{g}\mu_B S(S+1)}{3\gamma_I kT} \quad (2.20)$$

where A^{pc} from e.g. Eq. (2.18) is given by

$$A^{\text{pc}} = \frac{\mu_0}{12\pi} h\gamma_I \bar{g}\mu_B \left(\frac{g_{\parallel}^2}{\bar{g}^2} - \frac{g_{\perp}^2}{\bar{g}^2} \right) \frac{1}{r^3} (3 \cos^2 \theta - 1) \quad (2.21)$$

A of Eqs. (2.2) or (2.4), together with A^{pc} of Eq. (2.21), provide orientational average values of the hyperfine coupling tensor of Eq. (1.51).

2.2.2.2. Ligand-centered contributions

The first improvement of the dipole–dipole approximation is introduced by the consideration that the unpaired electron(s) is at least spread within the cage formed by the donor atoms. In the case of 4f electrons this does not produce a significant effect, whereas a 3d electron appears to the nucleus as a magnetic point-dipole only at large distances. An estimate of the lower limit of this distance is 700 pm [5]. In order to properly evaluate the pseudocontact term at shorter distances it is necessary to consider the appropriate MOs and to apply the dipolar interaction Hamiltonian to these wavefunctions. Attempts at this evaluation assuming a series of point multipoles instead of a simple point-dipole, with the aim of mimicking the electron distribution within the metal atomic orbitals, have been partially successful [6–8]. These considerations provide considerable corrections on nuclei close to the paramagnetic center. Nuclei far from the paramagnetic center still see the electron localized at the metal. Finally, if the electron is considered to be delocalized on the entire molecule, the problem is further complicated. Pseudocontact shift is also provided by spin density in a p orbital which has an orbital contribution to the magnetic moment different from zero. This is very relevant for heteronuclei like ^{15}N or ^{13}C which may bear unpaired spin density on p_z orbitals. The picture is of the type of Fig. 2.1 where, besides spin polarization, dipolar interactions occur. For example, fractions of unpaired electrons delocalized onto nitrogen p orbitals in $\text{Fe}(\text{CN})_6^{3-}$ are predicted to affect seriously the overall ^{14}N hyperfine shifts [9]. Therefore, the analysis of hyperfine shifts for heteronuclei requires ligand-centered pseudocontact shifts to be taken into account. Hydrogen nuclei have no accessible p orbitals and hence any ligand-centered effect can only arise from unpaired spin density on p_{π} orbitals of neighboring atoms. Thus, the effects are expected to be smaller, although not necessarily negligible.

2.3. Shift and spin patterns for protons and deuterons in solution

From the equations given so far, it is difficult to predict any behavior of chemical compounds from the hyperfine shift point of view. Still, any effort is welcome in providing rules and expectation under certain conditions. We will see here that this is somewhat possible.

Chemical bonds involving protons and deuterons are very similar to one another. Therefore, since the contact and pseudocontact shifts are independent of the nuclear parameters, the shifts are essentially the same. Both nuclei have the characteristic

that only 1s orbitals are involved. Therefore, protons and deuterons are discussed together. Sometimes, the use of ^2H NMR can be appropriate because it has a smaller linewidth than ^1H (see Section 3.9).

Let us first try to discuss the contact contribution to the shift for protons and deuterons. As we shall see, there are conditions under which the pseudocontact shifts are small, or can be factorized out. In the case of a monodentate ligand which exchanges rapidly from bound to free, the pseudocontact shift has a certain value when the ligand occupies a given coordination position and a different value when it occupies a different coordination position. The average in the absence of geometric constraints is zero. We have already seen that the hyperfine coupling constant is proportional to the spin density normalized to one electron. The proportionality constant depends on the magnetic properties of the two interacting particles. For the hydrogen atom such a constant K is experimentally found to be equal to $1.42 \times 10^9 \text{ Hz}$ [10]. In hydrogen and hydrogen isotopes (deuterium, tritium) there is only one pathway to generate contact spin density at the nucleus, i.e. through the 1s orbital, and no other orbital contributes to the contact or pseudocontact shift. The following equation then relates the contact hyperfine coupling with spin density:

$$\frac{A}{h} = \frac{K\rho}{2S} \quad (2.22)$$

where K for the other hydrogen isotopes (by recalling that A contains γ_I (Eq. (2.2)) and that $\sum_i \rho_i$ is the same for all isotopes) is given by ($i = 2, 3$)

$$K(^i\text{H}) = \frac{\gamma(^i\text{H})}{\gamma(^1\text{H})} K(^1\text{H}) \quad (2.23)$$

Let us now consider an organic radical, e.g. an alkane. The unpaired electron will be in a MO. If the alkane radical is negative, the electron will be in the *lowest unoccupied MO* (LUMO), if positive or neutral in the *highest occupied MO* (HOMO). The amount of unpaired electron directly delocalized at the hydrogen nucleus will be proportional to the coefficient representing its 1s orbital in the MO containing the unpaired electron. Furthermore, we may have spin polarization from the fraction of an unpaired electron in a p orbital of a carbon or nitrogen atom to the hydrogen 1s orbital. Typical examples of spin polarization will be discussed later.

When the unpaired electron in the molecule resides on a metal ion, spin delocalization on the ligand can occur through different mechanisms, and different signs of spin density can arise. Positive contributions to the spin density on the ligand arise from the MO(s) involving partially filled metal orbitals. The HOMO of the ligand which is involved in the MO together with the metal orbital bears a fraction of unpaired electron. Negative contributions occur through spin polarization from unpaired electrons in the atomic orbitals of the metal and doubly occupied MOs of the metal ligand complex.

The variety of spin density distributions on the same ligand by changing the metal ions depends on the different weights of the two above contributions. Spin density distributions can also change if σ and π mechanisms contribute to different extents.

Let us now consider the mechanism of spin delocalization in the water molecule when bound to a paramagnetic metal ion. Table 2.1 reports the proton A/h values for some hexaaqua metal complexes. They have been determined from hyperfine shifts, although sometimes they have been determined as absolute values from relaxation studies (see Chapter 3). Spin density has been evaluated through Eq. (2.22). The proton hyperfine shifts, assumed to be mainly contact in origin as a result of the averaged high symmetry, are downfield and the hyperfine coupling constants are positive. With the possible exceptions of Ti^{3+} , Fe^{3+} and Mn^{2+} , it appears that the hydrogen spin density, which is also listed in Table 2.1, tends to correlate with the number of unpaired t_{2g} electrons (Fig. 2.10). The t_{2g} orbitals have the correct symmetry for π bonding. Unpaired electrons in the e_g orbitals, which have the correct symmetry for σ bonding, do not affect the value of ρ , and indeed the experimental proton hyperfine coupling constants in Cu^{2+} (d^9) and Ni^{2+} (d^8) complexes, having

Table 2.1

Hyperfine coupling constants^a of water nuclei in aqua complexes of common metal ions

Metal ion	Electronic configuration	2S	n^b	$^1\text{H}A/h$ (MHz) ^c	$^{17}\text{O} A/h$ (MHz)	Reference
Ti^{3+}	d^1	1	1	4.5 (3.2×10^{-3}) ^d	4.4 ^d	[11,12]
VO^{2+}	d^1	1	1	2.1 (1.4×10^{-3}) ^d	3.8 ^d	[13,14]
V^{2+}	d^3	3	3	2.0 (4.2×10^{-3})		[15]
Cr^{3+}	d^3	3	3	2.0 (4.2×10^{-3})		[15,16]
Mn^{2+}	d^5	5	3	0.6–1.0 ($(2.2\text{--}3.5) \times 10^{-3}$)	5.3	[15,17,18]
Fe^{3+}	d^5	5	3	0.4–1.3 ($(1.4\text{--}4.6) \times 10^{-3}$)		[15,19]
Fe^{2+}	d^6	4	2		9.4	[17]
Co^{2+}	d^7	3	1	0.4 (1.1×10^{-3})	14.8–15.7	[16,17,20]
Ni^{2+}	d^8	2	0	0.2 (3×10^{-4})	20.4	[16,21]
Cu^{2+}	d^9	1	0	0.06–0.19 ($4.2 \times 10^{-5}\text{--}1.3 \times 10^{-4}$)	50.0	[16,22]
Ln^{3+}	$f^1\text{--}f^6, f^8\text{--}f^{13}$				0.6–0.8	[23]

^a Contact for protons; contact + ligand-centered pseudocontact for oxygen. Positive signs indicate downfield shifts for ^1H and upfield shifts for ^{17}O signals. ^b Number of unpaired electrons in t_{2g} orbitals for high-spin complexes with O_h symmetry. ^c ρ_{H} values in parentheses, estimated from Eq. (2.22). ^d Absolute values (obtained from relaxation data).

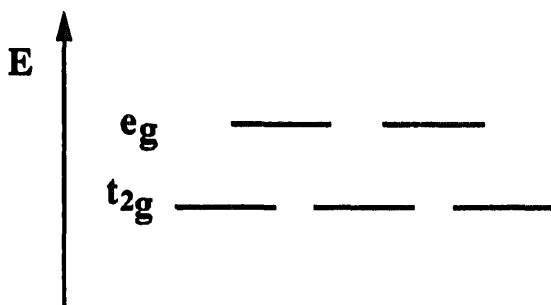


Fig. 2.10. e_g and t_{2g} orbitals in octahedral symmetry. The occupancy of t_{2g} orbitals for the various complexes is reported in Table 2.1.

no unpaired electrons in t_{2g} orbitals, are very small. It appears, therefore, that unpaired π electrons of the metal ions delocalize onto the H_2O moiety. One fully occupied water MO of σ type is capable of directly overlapping with the t_{2g} 3d orbital set of the metal. Thus the unpaired t_{2g} electron is capable of directly producing spin density on the protons. A further π interaction with the metal t_{2g} set arises from a non-bonding p orbital of oxygen, which would place spin density on the protons only through spin polarization. The sign of the observed shifts shows that the former mechanism is dominant [16]. The ^{17}O data (Table 2.1) show large hyperfine coupling constants when unpaired electrons are located in the e_g orbitals, which have the correct symmetry for σ bonding. The data for $Cu(H_2O)_6^{2+}$ and $Ni(H_2O)_6^{2+}$ demonstrate this clearly. It is obvious that direct delocalization through metal–oxygen σ bonding involving oxygen s orbitals gives rise to quite sizable spin density on the oxygen nucleus.

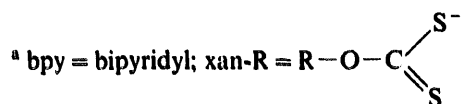
Let us now consider the complexes between amines (am) and nickel(II). The stoichiometry is $Ni(am)_6^{2+}$ and the geometry octahedral. The splitting of the d orbitals with the electron occupancy is analogous to that discussed for the hexaaqua complex (Fig. 2.10 and Table 2.1). The two e_g unpaired electrons will have an excess of $M_S = -\frac{1}{2}$ occupancy (positive spin density). Such $-\frac{1}{2}$ spin will be transmitted on the ligand through a MO which is a linear combination of the d orbitals and the ligand HOMO. The latter is mainly constituted by the atomic orbitals of the nitrogen atoms in accordance with the lone pair being localized on the nitrogen. The contribution to the ligand HOMO of atomic orbitals of the other ligand atoms decreases dramatically with the number of bonds. It follows that the spin density transmitted through this mechanism will rapidly decrease to zero as the number of chemical bonds between the metal and the resonating proton increases. The proton shifts fall rapidly to zero as we move away from the α -carbon [24,25]. The positive shift (in frequency) is due to $-\frac{1}{2}$ spin density (see Eqs. (2.6) and (2.22)), which in turn is the consequence of direct transfer with the same sign from d orbitals to ligand orbitals.

A second mechanism involving spin polarization may also be operative, in which spin polarization yields alternate positive and negative unpaired spin density along the ligand backbone. The protons bound to nitrogen experience negative shift, as is also observed in coordinated ammonia [26]. It is believed that it is due to prevailing spin polarization from a nitrogen p orbital to the hydrogen 1s orbital [25,26]. 1H , ^{13}C and ^{14}N shift values are available for ethylamine coordinated to a bis(acetylacetonate) nickel(II) complex [25]. It is reasonable to believe that the hyperfine shift is mainly contact in origin. The ^{14}N , $^{13}C_\beta$, and α -proton hyperfine couplings are positive (see Table 2.2), whereas α -carbons and amine protons have negative hyperfine couplings probably due to spin polarization. The spin polarization mechanisms which account for upfield shifts do provide a downfield mechanism for α -CH protons (see Section 2.4). It is possible that spin polarization and direct delocalization mechanisms are simultaneously operative. The contact shifts are negative for protons of ammonia coordinated to Cu^{2+} , Ni^{2+} and Co^{2+} [26] for the same mechanism as discussed above; the contact shifts are positive for Mn^{2+} owing to a dominant mechanism of direct transfer of spin density from t_{2g} orbitals to 1s hydrogen orbitals [26]. Table 2.2 also shows the hyperfine shifts (essentially contact, see later) in a

Table 2.2

Estimated A/n values (MHz) for ^1H , ^{13}C and ^{14}N nuclei of nitrogen- and sulfur-containing ligands of nickel(II)

Ligand								Reference
Ammonia		N^1H_3 –1.5						[26]
Ethylamine		^{14}N 14.4	N^1H_2 –2.64	$^{13}\text{CH}_2$ –0.70	C^1H_2 1.02	$^{13}\text{CH}_3$ 1.80	C^1H_3 0.22	[25]
(bpy)Ni(xan-R) ₂ ^a		$\alpha\text{-C}^1\text{H}$	$\beta\text{-C}^1\text{H}$	$\gamma\text{-C}^1\text{H}$	$\delta\text{-C}^1\text{H}$	$\varepsilon\text{-C}^1\text{H}$	$\zeta\text{-C}^1\text{H}$	[27]
	R							
	ethyl	–0.03	0.03					
	propyl	–0.03	0.04	0.02				
	butyl	–0.03	0.04	0.01	0.003			
	pentyl	–0.03	0.04	0.01	0	0.001		
	hexyl	–0.03	0.04	0.01	0	0	0	
	cyclo-hexyl	–0.23	0.09	0.005	0.001			
			0.01	0.001				
	R	$\alpha\text{-}^{13}\text{CH}$	$\beta\text{-}^{13}\text{CH}$	$\gamma\text{-}^{13}\text{CH}$	$\delta\text{-}^{13}\text{CH}$	$\varepsilon\text{-}^{13}\text{CH}$	$\zeta\text{-}^{13}\text{CH}$	
	ethyl	0.20	0.18					
	propyl	0.18	0.17	0.02				
	butyl	0.18	0.17	0.02	0.02			
	pentyl	0.18	0.17	0.02	0.02	0.004		
	hexyl	0.18	0.16	0.03	0.02	0.003	0.002	
	cyclo-hexyl	0.15	0.04	0.02	0.01			



nickel(II) bis(alkylxantate) complex with aliphatic chains of variable length [27]. The upfield shift of $\alpha\text{-CH}$ protons is due to spin polarization by π spin density in the delocalized xanthate ring [27].

The case of the hexa(pyridine) nickel(II) complex has been extensively debated in the early literature of NMR of paramagnetic complexes [28–32]. The shift pattern with $\alpha\text{-H} > \beta\text{-H} > \gamma\text{-H}$ (Fig. 2.11 and Table 2.3) was soon recognized to be predominantly of σ type. The ligand has a σ MO system which has the correct symmetry to overlap with the $d_{x^2-y^2}$ and d_{z^2} orbitals. However, spin polarization can induce $\frac{1}{2}$ spin density in the π system. Once some unpaired spin density is in a p_π orbital, it spin-polarizes the electrons of the $\text{C}-\text{H}$ σ bond, thus producing a further mechanism for transferring spin density on the proton.

If the spin delocalization mechanism were σ solely, substitution of $\gamma\text{-H}$ with $\gamma\text{-CH}_3$ would produce almost zero spin density on the $\gamma\text{-CH}_3$ protons. On the contrary (Table 2.3 and Fig. 2.11), some upfield (negative) shift is observed [34,35]. Spin polarization, from e.g. positive spin density on the p_z orbital of an sp^2 carbon, produces negative spin density on the attached proton (Fig. 2.12), and positive spin density again on the protons of an attached CH_3 moiety. Therefore, if the $\gamma\text{-CH}_3$ proton experiences upfield shift, it experiences $\frac{1}{2}$ spin density which comes from $\frac{1}{2}$

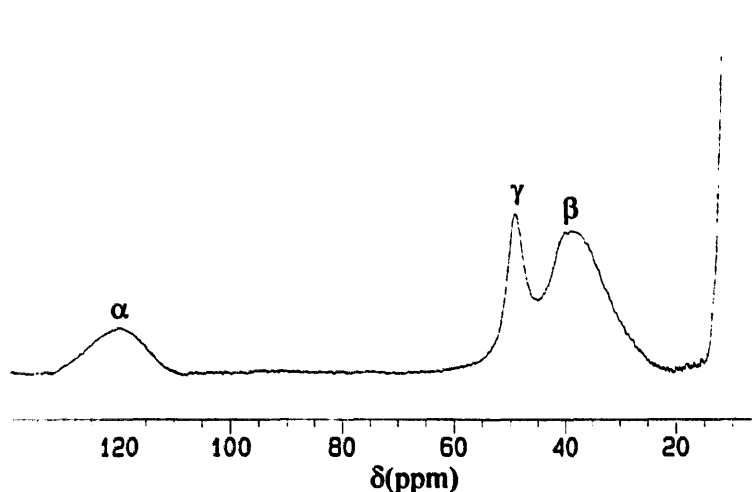


Fig. 2.11. ^1H NMR spectrum of hexa(pyridine)nickel(II). The shift pattern is $\alpha\text{-H} \gg \gamma\text{-H} > \beta\text{-H}$, indicating predominance of a σ -type mechanism with a π contribution.

Table 2.3

Estimated A/h values (MHz) for ^1H , ^{13}C and ^{14}N nuclei of pyridine and γ -picoline axially bis-coordinated to nickel(II) bis-acetylacetonate

Ligand		A/h (MHz)	Reference
Pyridine	^{14}N	+18	[33]
Pyridine	$\alpha\text{-}^{13}\text{C}$	-0.3	[34,35]
Pyridine	$\beta\text{-}^{13}\text{C}$	+0.7	[34,35]
Pyridine	$\gamma\text{-}^{13}\text{C}$	-0.1	[34,35]
γ -Picoline	$\gamma\text{-}^{13}\text{CH}_3$	+0.1	[35]
Pyridine	$\alpha\text{-}^1\text{H}$	+0.9	[36]
Pyridine	$\beta\text{-}^1\text{H}$	+0.3	[36]
Pyridine	$\gamma\text{-}^1\text{H}$	+0.35	[36]
γ -Picoline	$\gamma\text{-C}^1\text{H}_3$	-0.1	[35]

spin density of the p_z of the γ -carbon, which in turn comes from $-\frac{1}{2}$ spin density in the σ MO. Several calculations are available which try to factorize the various contributions.

In the case of pyridine bound to chromium(III), the three unpaired electrons sit in d_{xy} , d_{xz} and d_{yz} orbitals which do not overlap with ligand σ orbitals. Therefore, there is no mechanism for direct unpaired electron transfer onto the ligand. Spin density is produced in the doubly occupied ligand HOMO through spin polarization from the non-bonding d_{xy} , d_{xz} and d_{yz} orbitals. The spin and shift patterns in bis malonato bis pyridine chromium(III) are reversed with respect to the nickel case, with some tendency to alternation [37].

Imidazole ligands have been studied with iron, either $2+$ ($S=2$) or $3+$ ($S=\frac{1}{2}, \frac{5}{2}$), Co^{2+} , Ni^{2+} , Cu^{2+} [36,38,39]. The spectrum of $\text{Fe}(\text{NEtIm})_6^{2+}$ [38] is reported in Fig. 2.13. The shifts are downfield and the order, if all substituents are taken into

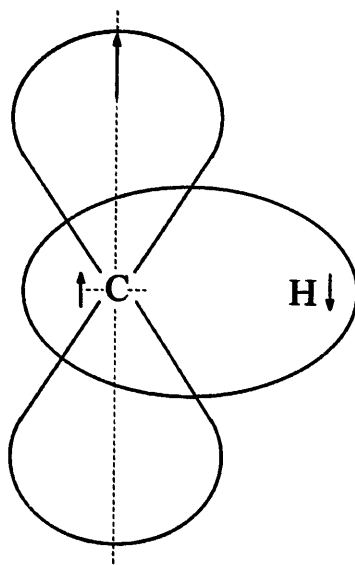


Fig. 2.12. The spin density on protons has the opposite sign of that on the attached sp^2 carbon.

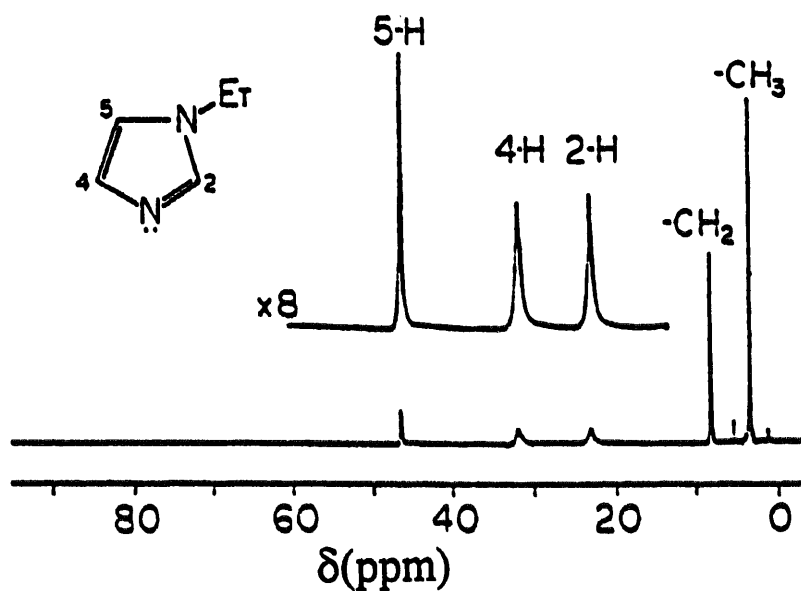


Fig. 2.13. ^1H NMR spectra of $\text{Fe}(\text{NEtIm})_6^{2+}$ [38].

account, is $\text{N}(1)\text{H} > 5\text{H} > 4\text{H} > 2\text{H} > \text{NCH}_3 \geq 5\text{CH}_3$. Probably this is the result of σ spin delocalization, π spin delocalization, and spin polarization effects. In the case of low spin iron(III), 2H is sizably upfield in $\text{Fe}(\text{CN})_5\text{Im}^{2-}$ (about 20 ppm), NCH_3 or 5CH_3 are downfield, and the other ring protons are slightly upfield. Alternation of proton and methyl shifts has been interpreted as due to a predominance of direct π spin density onto the imidazole ring [38].

Completely different is the shift pattern for pyridine-*N*-oxide in hexa(pyridine-*N*-oxide) nickel(II) [39–41] (Table 2.4). This is also a pertinent example of how spin

Table 2.4

Hyperfine shifts (ppm) of ring nuclei in octahedral complexes of Ni^{2+} with aniline and pyridine-*N*-oxide

Ligand		ortho	meta	para	Reference
Aniline	^1H	−6.9	+3.8	−7.6	[41]
Py-NO	^1H	−13	+11	−17	[38]
	^{13}C	+166	−65	+90	[40]

delocalization occurs in a six-membered π system. Here the *ortho* and *para* protons experience upfield shift, whereas the *meta* protons experience downfield shift. The absolute values of the hyperfine shifts are not sensitive to the distance from the paramagnetic center. This behavior could be accounted for by the non-orthogonality of the p_π of nitrogen with the M—O coordination bond (see also Section 2.4). The M—O coordination bond involves the e_g orbitals which have unpaired electrons. The unpaired electron in the p_z of nitrogen delocalizes into the ring through a π orbital of either bonding or antibonding character. If $\frac{1}{2}$ spin is present in a π MO orbital, it polarizes the doubly occupied π MOs. So, in any p_π of each carbon or nitrogen atom of the ring there is $\frac{1}{2}$ spin of the given MO and a tendency to have the same spin from the other π MOs through spin polarization. However, the total spin on every doubly occupied MO has to be zero. Therefore, if spin polarization causes $\frac{1}{2}$ spin contribution on a p_z orbital it has to cause $-\frac{1}{2}$ spin polarization of the same amount in absolute value on a p_z of another atom, in order to make zero spin density all over the six atoms per doubly occupied MO. As a result, total $-\frac{1}{2}$ spin density occurs at p_z of *ortho* and *para* carbons, whereas $\frac{1}{2}$ spin density occurs at p_z of *meta* carbons. Note that from the shifts the amounts of $-\frac{1}{2}$ and $\frac{1}{2}$ electron spins appear to be within a factor of two in absolute values.

A similar pattern is shown in d^5 – d^9 ions [41]. However, the ratios of the shifts varies with the metal ion. In the case of d^1 ions the shifts are very small, while in the case of Cr^{3+} the shifts are all downfield [39]. This possibly indicates that more mechanisms contribute to the overall shifts.

The amount of spin density transferred from a p_z of an sp^2 CH moiety to a proton is proportional to the amount of spin density on the p_z orbital itself through a proportionality constant which has been calculated to be about -70 MHz (Fig. 2.12 and see later). The proportionality constant for a proton of a free rotating CH_3 group bound to an sp^2 carbon is about $+75$ MHz (see later).

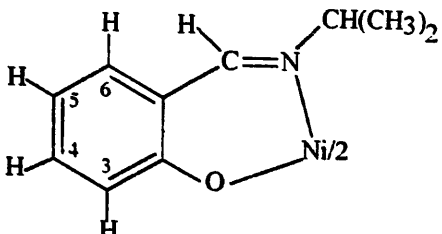
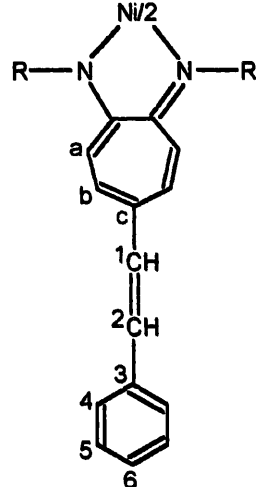
Phenylamine types of ligand behave like pyridine-*N*-oxide (Table 2.4) [41]. The same holds for phosphines [42]. It is also likely that phenolates are similar to the above systems.

When the number of atoms between the metal and the aromatic ring increases, like in $\text{Ph}-\text{C}=\text{N}-\text{R}$ [43], $\text{Ph}-\text{CONH}_2$ [41], Ph_3PO [44], $\text{Ph}-\text{CH}_2-\text{NH}_2$ [45], the patterns are similar to those described above but the shifts on the aromatic ring are about one order of magnitude smaller.

Other ligands like phenanthroline [46–48] and bipyridyl [49,50] are expected to behave similar to pyridine. Salicylaldiminates (Table 2.5) display two spin delocaliza-

Table 2.5

Estimated A/h values for protons in nickel(II) bis-salicylaldiminato and bis-aminotroponeiminato systems

Structure	Proton	A/h (MHz)	Reference
	3	-0.30^a	[51]
	4	$+0.30^a$	
	5	-0.29^a	
	6	$+0.14^a$	
	a	-1.29^b	[52]
	b	$+0.66^b$	
	(c)	(-1.80^b)	
	1	$+0.60^b$	[53]
	2	-0.87^b	
	4	-0.19^b	
	5	$+0.05^b$	
	6	-0.21^b	

^a Pseudocontact contributions to the hyperfine shifts have been factorized out. ^b Pseudocontact contributions to the hyperfine shifts have been neglected.

tion mechanisms: one through the oxygen atom and the other through the $-\text{C}=\text{NR}$ group, which is of minor relevance. The sum of the two mechanisms qualitatively accounts for the observed values (Table 2.5), although often a bias of negative shifts is observed [51,54].

Historically, bis(aminotroponeiminato) nickel(II) complexes have been thoroughly investigated. The compounds are either pseudotetrahedral or display a tetrahedral \rightleftharpoons planar equilibrium. The ligands contain seven-membered rings showing alternation of proton shifts and spin densities (Table 2.5). The interest lies in the variety of R derivatives which show how spin density can be transmitted through π bonds, whereas it cannot be transmitted through sp^3 carbons or through ethereal oxygen atoms [52,53].

NMR studies of porphyrin-containing iron complexes are very many owing to their importance in biological systems. The porphyrin systems are tetradentate dianionic ligands and essentially planar, as reported in Fig. 2.14. Iron can be in oxidation states varying from +2 to +4, and can also be magnetically coupled with a ligand cationic radical [55,56].

Iron(III) complexes are high spin when five-coordinated, or, if six-coordinated,

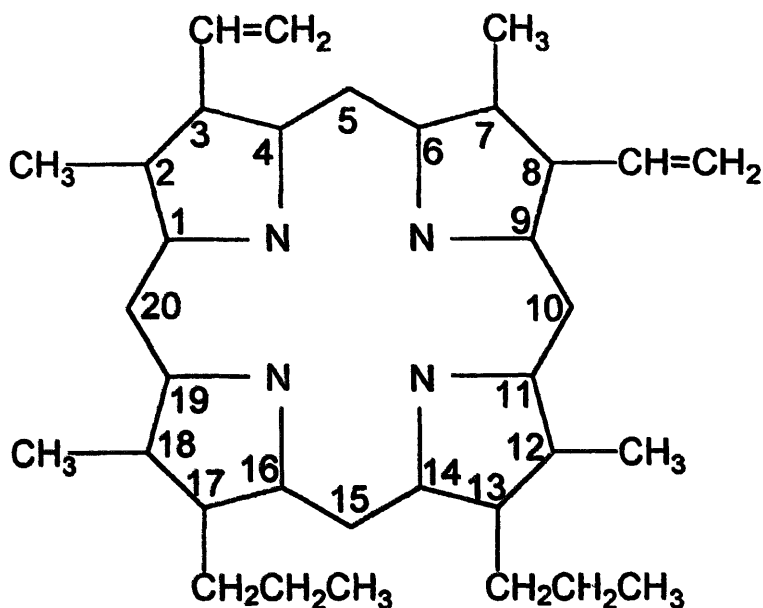


Fig. 2.14. Labeling of the positions in the porphyrin ring. The porphyrin shown is protoporphyrin IX.

when the axial ligands are relatively weak. The occupancy of the d orbitals is as shown in Fig. 2.15(A). The five electrons are spread over the five d orbitals with single occupancy. The ground state is an orbitally non-degenerate sextet. Spin orbit coupling causes the sextet spin level to be split at zero magnetic field (see Section 1.4) according to the scheme of Fig. 2.16. The large tetragonal component makes the above splitting relatively large. The larger the splitting, the faster the electron relaxation rate and the sharper the proton NMR lines (see Chapter 3) [57]. In five-coordinated complexes the order of the D value is $I^- \geq Br^- > Cl^- > NCS^- > F^-$

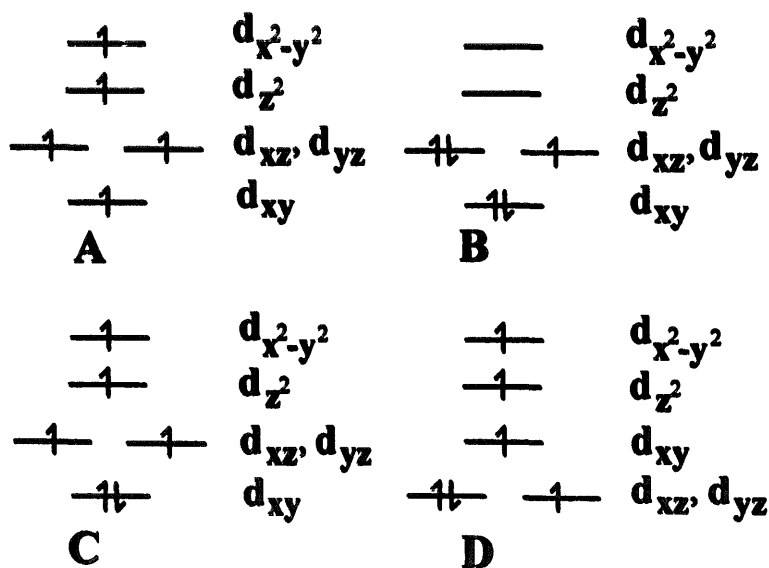


Fig. 2.15. d-orbital splitting in various iron(III) (A, B) and iron(II) (C, D) complexes of tetragonal symmetry.

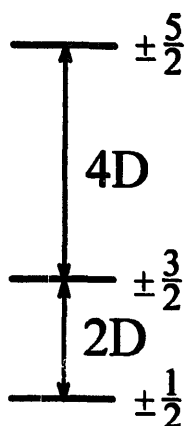


Fig. 2.16. ZFS of the spin sextet levels of high spin iron(III).

[58]. Typical values range from a few wavenumbers to ca. 15 cm^{-1} . Spin orbit coupling may also mix the $S = \frac{5}{2}$ ground state with the excited $S = \frac{3}{2}$ [59]. This is known in the literature as quantum mechanical spin admixing, which is reported to be relevant either in five-coordinated complexes or six-coordinated with very weak apical ligands [60].

The electron distribution of the d orbitals accounts for both σ and π spin density distribution on the porphyrin ring. In fact, whereas the $d_{x^2-y^2}$ orbital has the correct symmetry to form σ bonds, the d_{xz} and d_{yz} have the correct symmetry to give rise to π bonds. The σ spin density transfer mechanism accounts for the large downfield shifts of signals 2, 3, 7, 8, 12, 13, 17, 18 (numbering as in Fig. 2.14), or *pyrrole* signals (Fig. 2.17(A)). Consistently, CH_3 and CH_2 substituents in these positions are also downfield shifted. This is nicely shown in the proton NMR spectrum of FeTPPCl [61] (where TPP = 5,10,15,20-tetraphenylporphyrin) and of Fe(protoporphyrin IX dimethylester)Cl [62], as shown in Fig. 2.17. The protons of the phenyl groups at the 5, 10, 15, 20 (or meso) positions of FeTPPCl experience some alternating hyperfine shifts, which indicate that some π spin density is present on the phenyl rings as a result of a π spin density at the meso position. ^{13}C NMR data confirm the presence of π spin density of positive sign on the meso carbons [63]. Meso protons are generally downfield, especially in six-coordinated complexes (about 50 ppm) (Fig. 2.18(A)) [62]. In five-coordinated complexes the π contribution is relatively less important than the σ contribution and upfield shifts may occur (Fig. 2.18(B)) [64]. Such differences are ascribed to larger π delocalization contributions in six-coordinated complexes owing to the coplanarity of the metal with the ligand [62]. The presence of ZFS causes the occurrence of some pseudocontact shifts (Section 2.6) which will be discussed later.

Low spin iron(III) compounds have a d orbital occupancy as reported in Fig. 2.15(B). There is now only one unpaired electron in two degenerate orbitals of correct symmetry to give rise to π bonds. The unpaired electron appears to be delocalized into the $3e_\pi$ orbital of the porphyrin moiety [65]. The ^1H NMR spectrum of Fe(protoporphyrin IX)-imidazole-cyanide is reported in Fig. 2.19(A) [66]. The four methyls are all downfield, though to a quite smaller value than in the case of

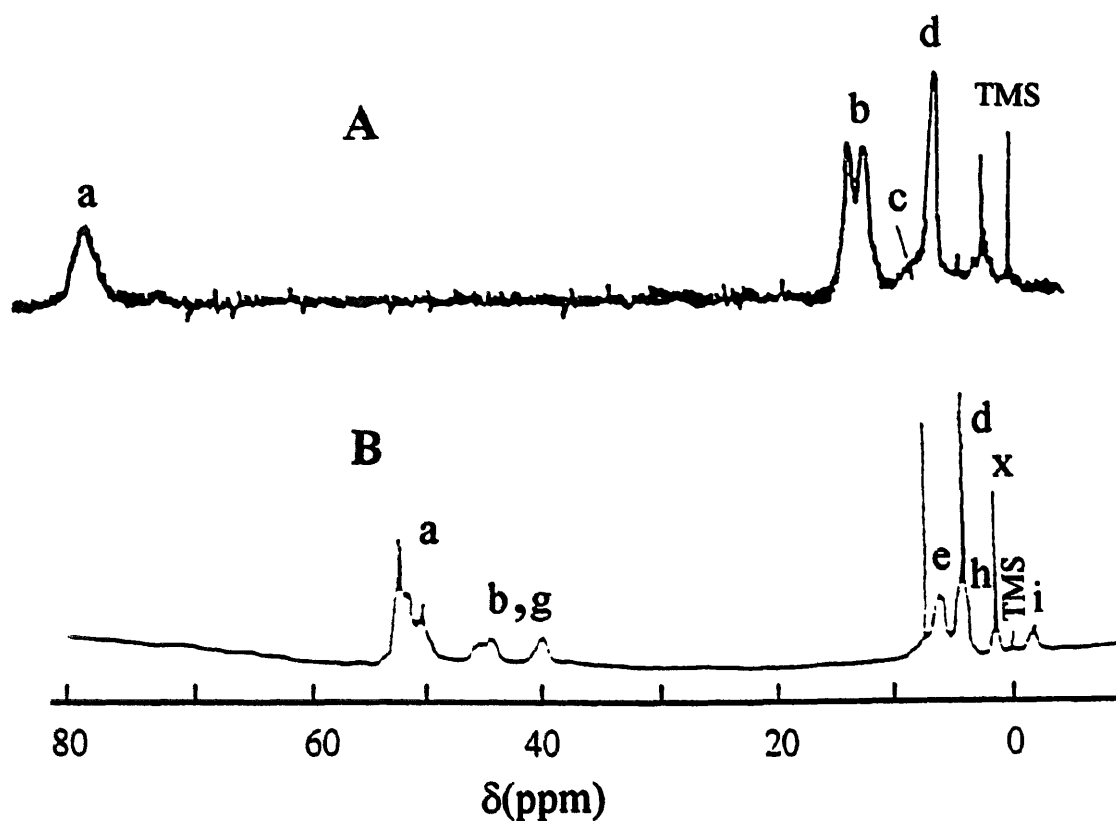


Fig. 2.17. ^1H NMR spectra of high spin Fe(III) porphyrins. (A) Fe TPP-Cl (no substituent at the pyrrole positions). Signal (a) refers to pyrrole protons; signals (b), (c) and (d) refer to the meta, ortho and para phenyl protons respectively [61]. (B) Fe (protoporphyrin IX)-Cl (see Fig. 2.14 for the ligand). Signals (a) belong to the methyl groups, signals (b) and (g) to the 13,17 $\alpha\text{-CH}_2$ and the 3,8 $\alpha\text{-CH}$; signals (d) to the COOH; signals (e) to the 13,17 $\beta\text{-CH}_2$; signals (h) and (i) to the 3,8 $\beta\text{-CH}$ cis and $\beta\text{-CH}$ trans respectively [62].

high spin iron(III) complexes. The metal-centered pseudocontact shifts have been factorized out through various procedures. An estimate for bis-imidazole systems is reported in Table 2.6 [67,68]. Now the pseudocontact shifts are larger than in the case of high spin iron(III). In proteins, the apical ligand is fixed and removes the degeneracy of the d_{xz} and d_{yz} orbitals, thus introducing large anisotropy in the peripheral substituents of the heme ring. In Fig. 2.19(B) the spectrum of metmyoglobin-cyanide is reported, with the assignment [69]. The splitting of the d_{xz} and d_{yz} orbitals can be as large as several times kT . When it is of the order of kT , the temperature dependence should take into account the Boltzmann population of the excited level, and even antiCurie behavior may be observed [70].

Iron(II) can be paramagnetic with four ($S = 2$) or two ($S = 1$) unpaired electrons, depending on whether it is five- or four-coordinated. In the former case, the orbital occupancy can be either one of the two schemes (C) and (D) of Fig. 2.15. In every case a predominance of σ delocalization is expected as well as moderate π delocalization at the meso positions [71]. A spectrum is reported in Fig. 2.20 [71]. In proteins, the position of the axial histidine ring determines the inequivalence of

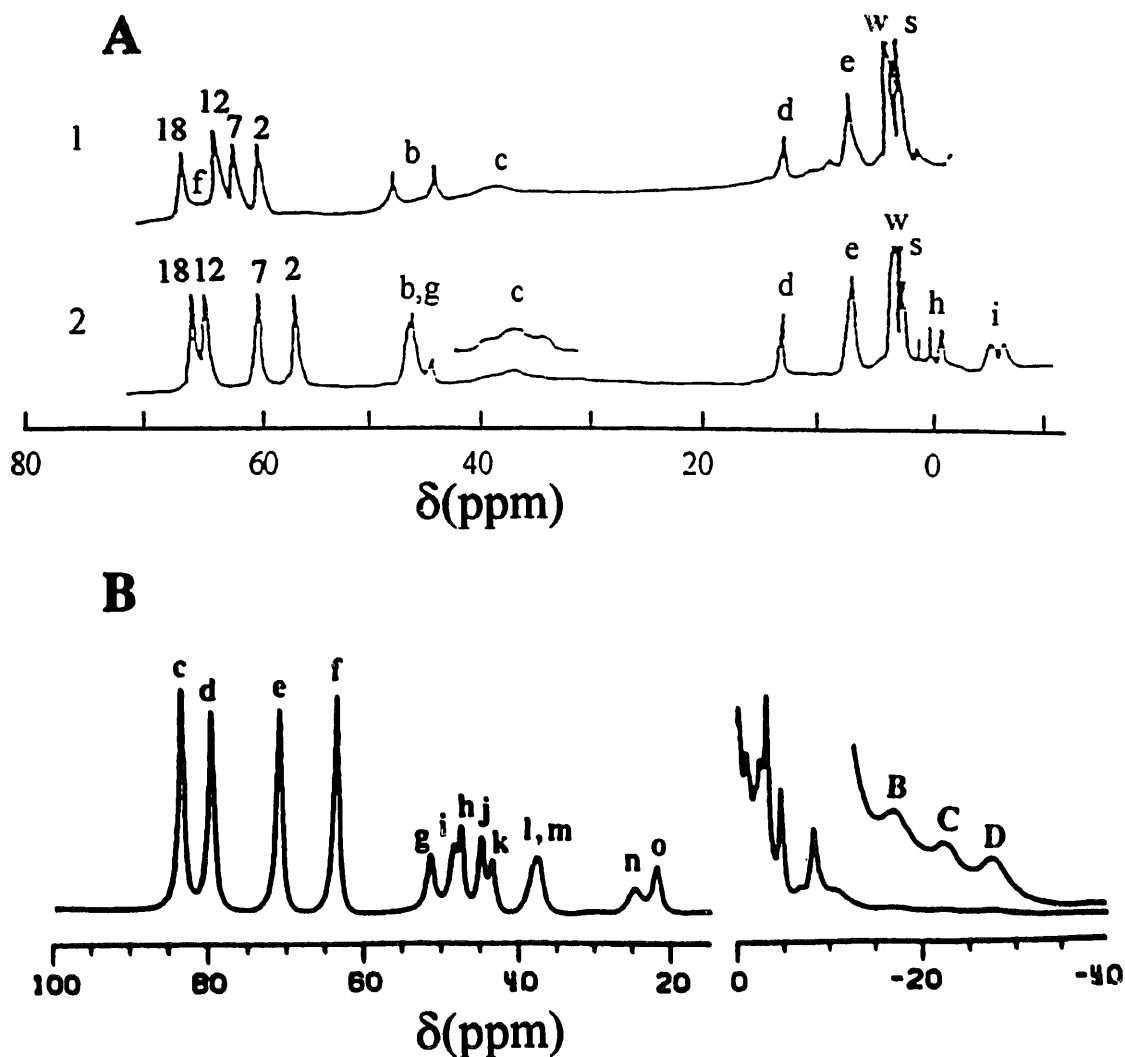


Fig. 2.18. ^1H NMR spectra of (A) six- and (B) five-coordinated iron(III) porphyrins. (A) 1 = 3,8-H; 2 = 3,8-vinyl porphyrin IX (Fig. 2.14). Numbers 2, 7, 12, 18 refer to methyl positions on the heme; (b) refers to 13- and 17-propionate $\alpha\text{-CH}_2$ signals; (c) to the 5, 10, 15 and 20 protons; (d) to the COOH protons; (e) to the 13,13 propionate $\beta\text{-CH}_2$ signals; (f) to the 3,8 H. (g) to the 3,8 $\alpha\text{-CH}$; (h) to the 3,8 $\beta\text{-CH}$ cis; (i) to the 3,8 $\beta\text{-CH}$ trans. (B) Cytochrome c' from *R. palustris*, pH 5. Signals (c)–(f) belong to porphyrin IX methyl groups, and upfield signals (B)–(D) to meso protons.

protons in the porphyrin plane. Probably as a result of this, a variety of patterns is observed with either one or two of the four metal substituents of protoporphyrin IX being downfield [69,73–75]. In the case of an $S = 1$ ground state, the contact shifts are dominated by π delocalization [76].

A comment is due to the spin patterns of the imidazole ring, which often is an axial ligand of hemes. In high spin iron(III) complexes and in high spin iron(II) complexes the shifts are far downfield, indicating a predominance of σ spin distributions. This is consistent with the presence of a single occupancy of the d_{z^2} orbital. On the contrary, in low spin iron(III) complexes the shifts of the histidine protons

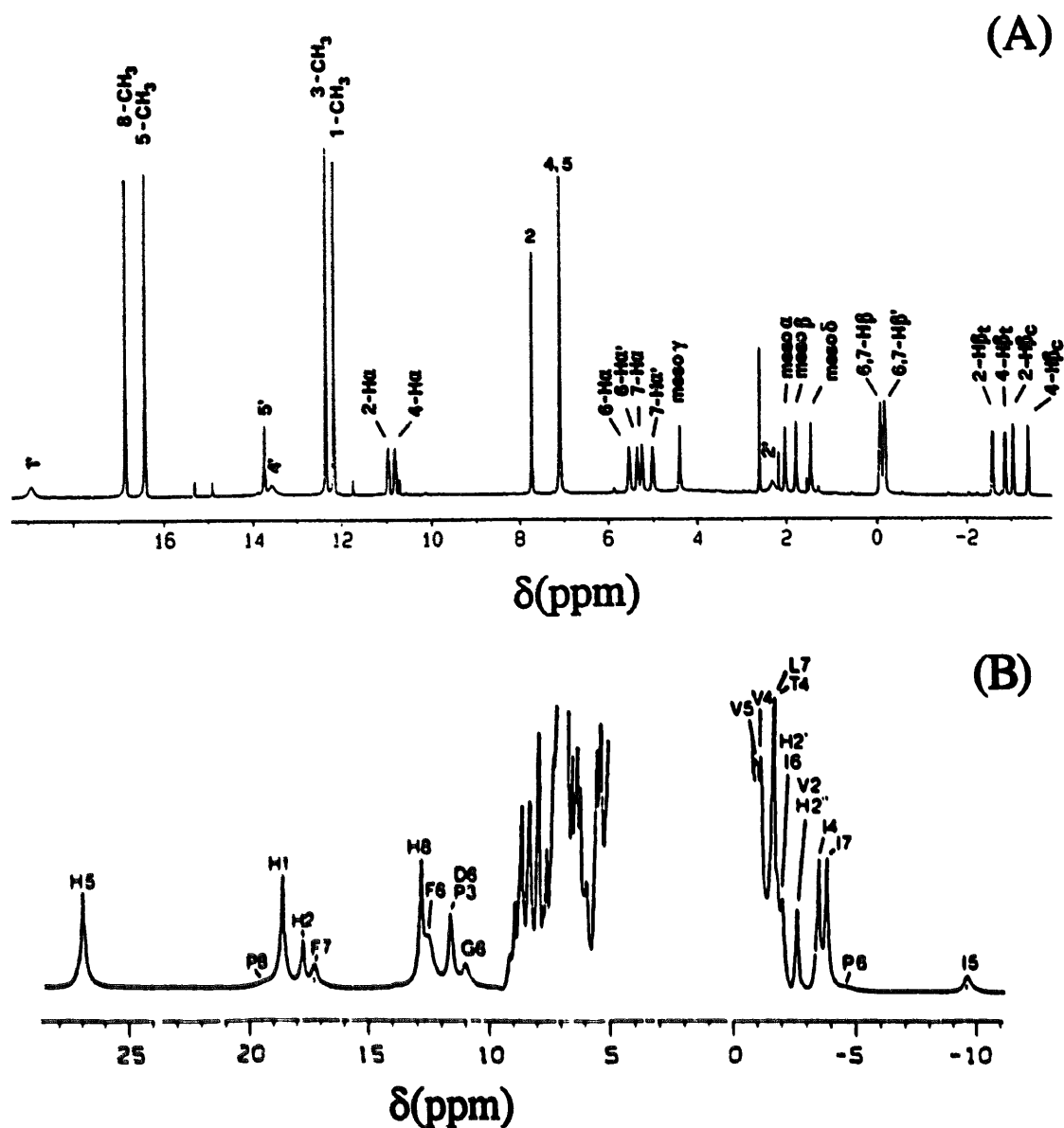


Fig. 2.19. ¹H NMR spectrum of Fe(protoporphyrin IX)-imidazole-cyanide (A) [66] and of metmyoglobin-cyanide (B) [69]. The assignment of the heme signals of the latter is as follows: H5 = 12-CH₃; H1 = 2-CH₃; H2 = 3-H α ; H8 = 18-CH₃; H2' = 3-H β cis; H2'' = 3-H β trans [69].

in ortho-like positions may be upfield to an extent which depends on the strength of the iron–imidazole bond [77].

2.4. Proton hyperfine coupling and conformation

The contact hyperfine shift contains information on conformational arrangements because it is somehow related to chemical bonds. The information, however, is generally hidden. In some cases, some relationships hold. For example, if we have a

Table 2.6

Factorization of contact and pseudocontact shifts in low spin bis-imidazole iron(III) porphyrins [67,68]

Position	Hyperfine shift (ppm)	Pseudocontact shift (ppm)	Contact shift (ppm)
<i>Heme</i>			
Meso <i>o</i> -H ^a	−3.09	−3.09	0
Meso <i>m</i> -H ^a	−1.49	−1.44	≈0
Meso <i>p</i> -H ^a	−1.37	−1.27	≈0
Meso <i>p</i> -CH ₃ ^b	−0.94	−0.94	0
Pyrrole H ^{a,b}	−25.4	−5.8	−19.5
Meso α-CH ₂ ^c	0.6	−4.5	5.1
Meso H ^d	−7.0	−9.3	2.3
Pyrrole α-CH ₂ ^d	2.0	−3.2	5.2
<i>Axial imidazole</i>			
1-H ^a	≈2	−9.6	11.6
1-CH ₃ ^c	17.2	10.3	6.9
2-H ^a	−9.5	−28.0	18.5
2-CH ₃ ^c	≈12	≈12	≈0
4-H ^a	9.7	−8.2	17.9
5-H ^a	4.0	−7.6	11.6
5-CH ₃ ^c	15.5	9.0	6.5

^a For Fe 5,10,15,20-tetraphenylporphyrin-(Im)₂⁺. ^b For Fe 5,10,15,20-tetratoluyllporphyrin-(Im)₂⁺. ^c For Fe 5,10,15,20-tetrapropylporphyrin-(Im)₂⁺. ^d For Fe 2,3,7,8,12,13,17,18-octaethylporphyrin-(Im)₂⁺. ^e For Fe 5,10,15,20-tetraphenylporphyrin-(CH₃Im)₂⁺.

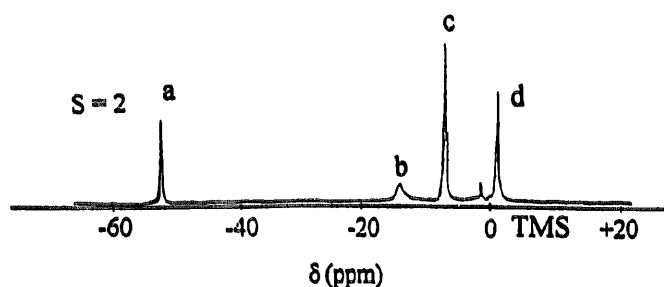


Fig. 2.20. ¹H NMR spectrum of *S* = 2 Fe 5,10,15,20-tetraphenylporphyrin (2-CH₃Im) [72]. a = 2,3,7,8,12,13,17,18-H; b = 2-CH₃Im 4,5-H; c = phenyl *ortho*-, *meta*- and *para*-H; d = 2-CH₃ImCH₃.

CH moiety of an sp³ carbon bound to an sp² carbon which bears spin density in the p_z orbital, a mechanism to originate spin density at the proton is the direct overlap between the sp² carbon p_z and the 1s hydrogen orbital [78] (Fig. 2.21). Such overlap depends on the dihedral angle θ between the p_z—C—C plane and the C—C—H plane (Fig. 2.21). The relationship, due to Karplus [79], is of the type

$$\frac{A}{h} = (a \cos^2 \theta + b \cos \theta + c) \frac{\rho_C^\pi}{2S} \quad (2.24)$$

where ρ_C^π is the spin density on the p_z orbital and *a*, *b* and *c* are constants. When

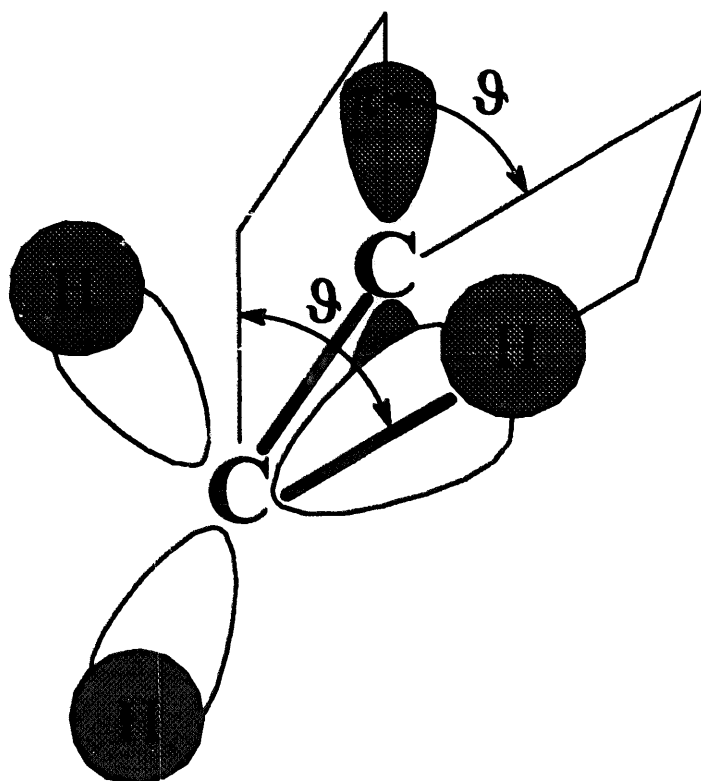


Fig. 2.21. CH moiety of an sp^3 carbon bound to an sp^2 carbon, illustrating the definition of the dihedral angle θ .

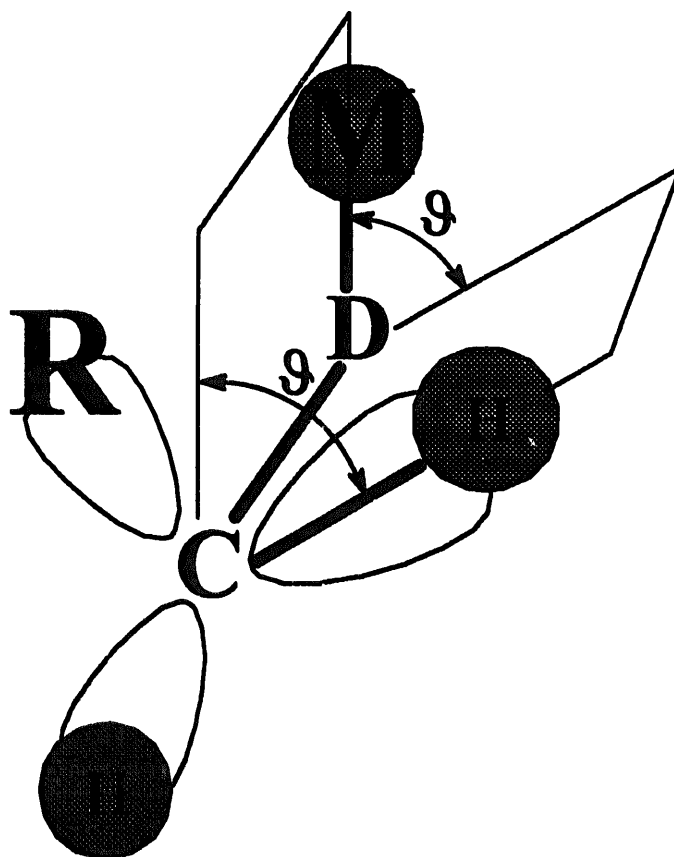
$\theta = 90^\circ$, $A/h = c\rho_C^\pi/2S$ and the spin transfer occurs only through the C–C–H σ bonds. b and c are usually small, a is about 140 MHz [78,79]. When the CH moiety belongs to a CH_3 group and the group is free to rotate, an average over all positions should be calculated. The average value of $a \cos^2 \theta$ is 75 MHz [78]. In other words, if there is a positive ($-\frac{1}{2}$) spin density on the sp^2 carbon atom, a positive spin density (scaled down by a factor 19 with respect to the K value of the hydrogen atom (Eq. (2.22))) is present on average on a proton of a CH_3 group, whereas it would be about -70 MHz (i.e. negative and scaled by a factor 20) if the proton were directly attached to the sp^2 carbon atom. Such scaling factors are the ratio between K of Eq. (2.22) and a parameter Q which relates the contact coupling constant of a given proton with the π spin density of an attached sp^2 carbon (Table 2.7) [80–83].

This reasoning induces one to think that, even in a moiety of the type M–D–C–H, where D is the donor atom, the CH proton experiences a contact coupling depending on the orientation of the D–C–H plane (Fig. 2.22). If the spin density is along the M–D bond, then the coupling depends on the dihedral angle between the M–D–C and D–C–H plane in a fashion similar to Eq. (2.22) (Fig. 2.21), θ being now defined with respect to the M–D bond rather than with respect to a non-bonding p_z orbital as in Fig. 2.21. This is the case when D is an amino nitrogen. This spin delocalization mechanism adds up to that described in

Table 2.7

 Q values (MHz) for fragments involved in π electron spin delocalization systems

Q_{CH}^{C}	Q_{CH}^{H}	$Q_{\text{CC}'}^{\text{C}}$	$Q_{\text{C}'\text{C}}^{\text{C}}$	$\langle Q_{\text{CCH}_3}^{\text{H}} \rangle$	Q_{CF}^{F}	Q_{FC}^{F}	Reference
+54.6	−65.8	+40.3	−39.0				[80]
	−75.6	+53.2					[81]
				+75			[82]
					−410	+2370	[83]

Fig. 2.22. Dihedral angle θ between the $\text{M}-\text{D}-\text{C}$ plane and the $\text{D}-\text{C}-\text{H}$ plane of $\text{M}-\text{D}-\text{C}-\text{H}$ moieties.

Section 2.3 for nickel(II) amine complexes. If the spin density is in a p orbital of the D atom orthogonal to the $\text{M}-\text{D}$ bond, a dependence on $\sin^2 \theta$ is more appropriate. This seems to be the case for S as donor atom [84].

2.5. The origin of the shifts in heteronuclei

If spin polarization and direct delocalization contributions to the shift make the predictions of the proton shifts difficult, the prediction is almost impossible in the

case of heteroatoms. In the case of σ spin density like in an aliphatic amine (Table 2.2(A)), the ^{13}C Fermi contact shift for the α -carbon of the aliphatic amine is upfield (A/h is negative) because of predominant spin polarization effects, whereas that for other carbon atoms is downfield, and rapidly attenuates with the number of bonds. A sizable downfield shift is experienced by the ^{14}N nucleus when nitrogen is a donor atom. In general, unpaired electrons in non-s orbitals of heteroatoms produce a further shift, dipolar in origin, which represents another unknown (see Section 2.2.2).

More hints are available for aromatic moieties. If we consider an sp^2 carbon atom bound to two more sp^2 carbon atoms in a delocalized moiety (e.g. in an aromatic ring), and we assume that unpaired spin density resides in the p_z orbitals, we have the following contributions to the contact interaction at the central carbon atom [85]:

- (1) spin polarization from the p_z orbital on the $2s$ orbital of the same atom (Fig. 2.23(A));
- (2) spin polarization from the p_z orbital on the $1s$ orbital of the same atom (Fig. 2.23(B));
- (3) spin polarization from the p_z orbitals of the side atoms on the $2s$ orbital of the central atom through the sp^2 σ bond (Fig. 2.23(C)).

The proportionality constant between unpaired electrons on the p_z orbital and the spin density on the $2s$ orbital of the same nucleus is of positive sign (Fig. 2.23(A)) and is between 40 and 50 MHz (Table 2.7). The proportionality constant from the

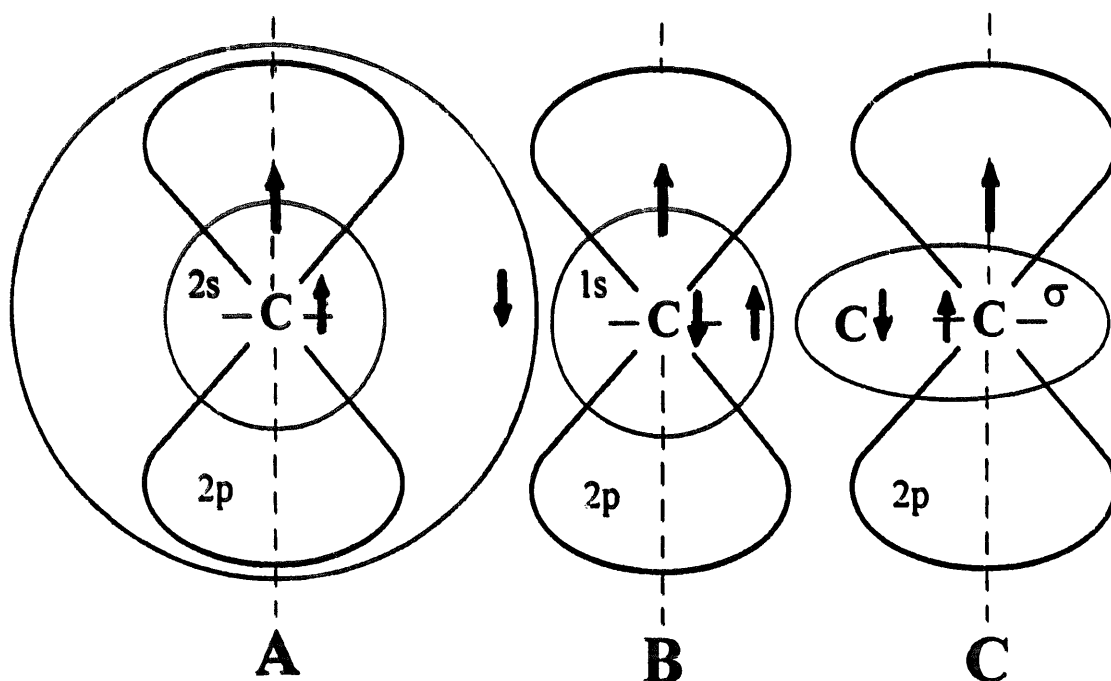


Fig. 2.23. Spin polarization mechanisms arising from unpaired spin density on a $2p_z$ orbital, illustrated for a ^{13}C nucleus. (A) Polarization through a $2s$ orbital; (B) polarization through a $1s$ orbital; (C) polarization on a nearby carbon through a σ bond.

unpaired spin density on the p_z orbital of the nearby carbon atom is negative (−39 MHz, Fig. 2.23(C)), and of the same sign as the polarization effect on the 1s orbital (−35 MHz, Fig. 2.23(B)).

From the foregoing analysis, it appears that there is more than one term making a significant contribution to the hyperfine coupling constant. The polarization of the 1s electron produces a somewhat larger spin density at the nucleus which is proportional, but opposite in sign, to the π spin density. The contribution from polarization of the three σ bonds by π spin density on the same atom has the same sign as ρ_C^π , because $Q_{CC'}^C$ are positive (Fig. 2.23(C) and Table 2.7). Finally, there is the polarization of the three σ bonds by π electron spin density on adjacent atoms, which is again a contribution opposite in sign to ρ_C^π because $Q_{C'C}^C$ is negative (Table 2.7 and Fig. 2.23(C)). The final value of the hyperfine coupling constant is therefore the result of considerable cancellation among the various contributions. In general the ρ_C^π values are determined from the ^1H Fermi contact shifts through the following equation

$$\frac{A}{h} = Q \frac{\rho_C^\pi}{2S} \quad (2.25)$$

which, analogously to Eq. (2.22), relates the contact hyperfine constant with a spin density. Of course, something similar holds for sp^2 nitrogen. It appears that, even considering the shift of the proton attached to the heteronucleus, the number of parameters is larger than the two experimental shifts. A deeper insight can be achieved by using experimental data on nuclear relaxation (see Section 3.9).

^{13}C data are available on several ligands. In Tables 2.3 and 2.4 the relative ^{13}C hyperfine shifts of pyridine and pyridine-*N*-oxide are reported [34,40]. In both cases it appears that there is alternation in the shifts, which would indicate π spin delocalization. However, the ratio between the shifts of protons and carbons at each position are different one from the other, and differ from what would be expected on the basis of a simple spin polarization mechanism. It is concluded that more than one mechanism is operative.

Data are available on ^{13}C and ^{15}N of cyanide bound to a heme moiety. Cyanide is the most common reactant employed to modify the heme moiety [86]. All the monocyano and dicyano derivatives of isolated porphyrins and hemoproteins are low spin and contain either diamagnetic iron(II) or paramagnetic ($S = \frac{1}{2}$) iron(III). ^{13}C and ^{15}N NMR spectra have been reported for the latter systems and, as shown in Tables 2.8 and 2.9, dramatic paramagnetic effects have been measured for both nuclei: the ^{13}C hyperfine shifts range from −2000 to −2400 ppm upfield [87] whereas the ^{15}N shifts range from 600 to 1200 ppm downfield [88–91]. The spin delocalization would be dominantly spin polarization through an $\text{Fe}-\text{C}$ π bond, which may also account for the opposite sign of carbon and nitrogen shifts. Possible metal-centered pseudocontact contributions estimated from the known metal-nucleus distance and magnetic anisotropy values are of the order of 100 to 300 ppm downfield. Theoretical studies [90] have estimated sizable ligand-centered pseudocontact contributions to the shifts of nitrogen in $\text{Fe}(\text{CN})_6^{3-}$ (Section 2.2.2).

Table 2.8

^{13}C chemical shifts (ppm from TMS) for coordinated cyanide in low spin iron(III) porphyrins and hemoproteins [87]

Iron species	Porphyrin 3,8-R group	^{13}C chemical shift
Fe protoporphyrin IX	$-\text{CH}=\text{CH}_2$	–2393
Hemin c	$-\text{CH}(\text{CH}_3)\text{SCH}_2-$ $\text{CH}(\text{NH}_2)\text{COO}^-$	–2300
Fe 3,8-disulfonate-deuteroporphyrin IX	$-\text{SO}_3^-$	–2167
Fe 5,10,15,20 tetra(4-carboxyphenyl)-porphyrin		–1968
($\text{C}_2\text{H}_5\text{NC}$)-myoglobin (diamagnetic)		171.3

Table 2.9

^{15}N chemical shifts (ppm from $^{15}\text{NO}_3^-$) for coordinated cyanide in low spin iron(III) porphyrins and hemoproteins

Iron species	Solvent	^{15}N chemical shift	Reference
Hemin	Me_2SO	732	[88]
	Py	696	
	CH_3OD	506	
	$\text{CH}_3\text{OD} + \text{D}_2\text{O}$ (1:1)	480	
	H_2O	448	
(4-AcPy)hemin	4-ACPy + D_2O	945	[88]
(Py)hemin	Py + D_2O	989	[88]
(3,5-Lu)hemin	3,5-Lu + D_2O	1070	[88]
(1- CH_3Im)hemin	1- CH_3Im + D_2O	926	[88]
Myoglobin	D_2O	931–948 ^a	[88]
Cytochrome c	D_2O	841	[89]
Hemoglobin	D_2O	975 (α)	[90]
		1047 (β)	
Horseradish peroxidase	D_2O	576	[91]
Cyt c peroxidase	D_2O	587	[91]
Lignin peroxidase	D_2O	608	[91]
Manganese peroxidase	D_2O	639	[91]

^a Depending on pH.

Although the magnitude of the shifts is only slightly sensitive to variations in the nature of the heme and to its contacts with the surrounding protein, it is strongly dependent on the identity of the trans ligand. For example, the ^{15}N signal in protohemin cyanide shifts from 945 to 989 to 1070 ppm downfield on passing from 4-acetylpyridine to pyridine to 3,5-lutidine as the trans ligand [89]. Both ^{13}C and ^{15}N hyperfine shifts are also very sensitive to changes in the solvent. Aprotic solvents usually give the largest absolute values, which decreases by as much as 200 ppm on passing from DMSO to methanol to water [88,89]. In general, the axial ligand field

strength of cyanide, and hence the extent of unpaired spin delocalization, decreases with the increasing hydrogen bonding capabilities of the solvent.

^{15}N NMR data are available for cyanometmyoglobin, cytochrome c, cyanomethemoglobin, and some peroxidases (Table 2.9) [88–91]. The large observable differences may be related to the different coordination strength of the trans histidine and/or to the different hydrophobicity of the CN binding site. The difference in the ^{15}N chemical shift (about 70 ppm) of the α and β subunits in hemoglobin (Table 2.9) [90] illustrates the sensitivity of the cyanide nuclei to the protein environment around the axial positions.

For ^{19}F Fermi contact shift of fluorine bound to sp^2 carbon atoms, spin density on the nucleus arises from spin polarization by ρ_{C}^{π} , as for analogous CH moieties, and from spin polarization by ρ_{F}^{π} , which occurs via direct delocalization through C–F π bonding (Fig. 2.24). The hyperfine coupling is therefore

$$\frac{A}{h} = Q_{\text{CF}}^{\text{F}} \rho_{\text{C}}^{\pi} + Q_{\text{FC}}^{\text{F}} \rho_{\text{F}}^{\pi} \quad (2.26)$$

where Q_{CF}^{F} is analogous to Q_{CH}^{H} or Q_{CC}^{C} and is negative, and Q_{FC}^{F} , which is the polarization effect of ρ_{F}^{π} on the C–F σ bond, is positive by analogy to Q_{CC}^{C} (see Table 2.7).

^{31}P contact shifts in ligands coordinating through P–O moieties in oxovanadium(IV), cobalt(II) and nickel(II) complexes are downfield and of the order of 10^3 ppm [92–94]. Smaller downfield shifts are observed for nickel-coordinated P–S moieties [95]. Direct P–M coordination gives rise to even larger hyperfine coupling than in P–O moieties. In low spin cobalt(II) complexes A/h values of the order of 10^2 MHz are found [96].

2.6. When is metal-centered pseudocontact shift expected

Pseudocontact shift is expected everytime there are energy levels close to the ground state. This causes orbital contributions to the ground state, and such contribu-

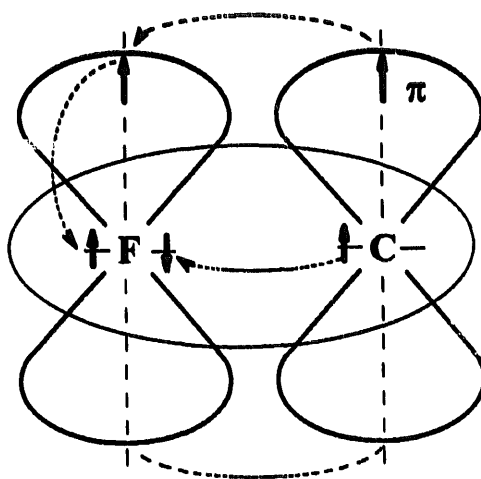


Fig. 2.24. Spin polarization (through σ bonding) and direct delocalization (through π bonding) mechanisms for unpaired spin density transfer from an sp^2 carbon to a fluorine nucleus.

tions are orientation dependent. Therefore, the magnetic susceptibility tensor is anisotropic. Anisotropy of the magnetic susceptibility tensors arises also from sizable ZFS of the S manifold (Section 1.4).

Six-coordinated high spin cobalt(II) in pure octahedral symmetry has a ${}^4T_{2g}$ ground state which is triply degenerate. Under spin–orbit coupling and low symmetry components up to six Kramers doublets can be obtained (Fig. 2.25) within 1000 cm^{-1} . The orbital contribution to the magnetic susceptibility is sizable, and the orbital contribution is intrinsically anisotropic. The pseudocontact shifts estimated [97] for a tetragonal complex are reported in Table 2.10. Octahedral nickel(II) complexes have a ${}^3A_{2g}$ ground state which is orbitally non-degenerate, with the first excited state at about $10\,000\text{ cm}^{-1}$. So, to a first approximation, its effects on the magnetic susceptibility tensor can be neglected.

It is foreseeable that pseudocontact shifts occur in low spin iron(III) porphyrins which in octahedral symmetry would have an orbitally triply degenerate ground state. Therefore, g and χ values in iron porphyrins are highly anisotropic (see Section 2.3) [67,68].

High spin iron–porphyrin systems have $S = \frac{5}{2}$ and are orbitally non-degenerate. The large tetragonal distortion induces a ZFS of the sextet as shown in Fig. 2.16, with D of the order of 10 cm^{-1} . The principal susceptibility values can then be

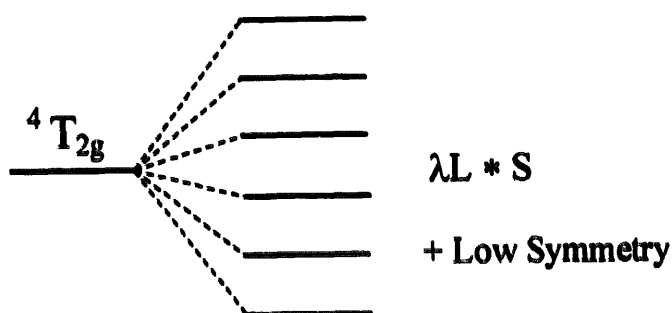


Fig. 2.25. A 4T state is split into six Kramers' doublets by spin orbit coupling and low symmetry components.

Table 2.10

Hyperfine (δ^{hyp}) and pseudocontact (δ^{pc}) shifts^a of the ${}^1\text{H}$ and ${}^{13}\text{C}$ nuclei of pyridine bis-coordinated to cobalt(II) bis-acetylacetonate [97]

Atom	δ^{hyp}	δ^{pc} (ppm)
$\alpha\text{-H}$	+ 32.9	– 39.5
$\beta\text{-H}$	+ 5.0	– 18.1
$\gamma\text{-H}$	– 9.4	– 15.6
$\alpha\text{-C}$	– 199	– 92.5
$\beta\text{-C}$	+ 229	– 35.7
$\gamma\text{-C}$	– 73.8	– 28.3

^a Pseudocontact shifts are estimated using single-crystal magnetic susceptibility data.

calculated through the Van Vleck equation (Eq. (1.40)), as long as $2D$ is larger than the Zeeman energy.

$$\chi_{zz} = \mu_0 \frac{g_{\parallel}^2 \mu_B^2}{4kT} \left[\frac{1 + 9 \exp(-2X) + 25 \exp(-6X)}{1 + \exp(-2X) + \exp(-6X)} \right] \quad X = \frac{D}{kT} \quad (2.27)$$

$$\chi_{xx} = \chi_{yy} = \mu_0 \frac{g_{\perp}^2 \mu_B^2}{4kT} \left[\frac{9 + \frac{8}{X} - \frac{11}{2X} \exp(-2X) - \frac{5}{2X} \exp(-6X)}{1 + \exp(-2X) + \exp(-6X)} \right] \quad (2.28)$$

By substituting the magnetic susceptibility values in Eq. (2.14) with expressions (2.27) and (2.28), and taking $\exp X = 1 + X$ ($D \ll kT$), the following equation is obtained [98].

$$\delta_{pc} = \frac{\mu_0}{4\pi} \frac{35\mu_B^2(g_{\parallel}^2 - g_{\perp}^2)}{36kT} \frac{3 \cos^2 \theta - 1}{r^3} \times \left[1 - \frac{32(g_{\parallel}^2 + \frac{1}{2}g_{\perp}^2)}{15(g_{\parallel}^2 + g_{\perp}^2)} \frac{D}{kT} \right] \quad (2.29)$$

This equation gives the sum of the magnetic susceptibility contributions of each state i , weighted by the population according to the Boltzmann distribution. Note the T^{-2} dependence of the pseudocontact shifts.

2.7. Attempts to factorize contact and pseudocontact shifts

As a result of the nature of the pseudocontact shifts, a knowledge of the magnetic susceptibility tensor provides a method for their independent evaluation, if it is assumed that the shifts are metal-centered dipolar in origin. In principle, therefore, by performing magnetic susceptibility measurements on single crystals with several orientations of the magnetic field, it is possible to determine the magnetic anisotropy and the principal axes of the magnetic tensor. By knowing the geometrical coordinates, the pseudocontact shifts can be easily predicted using Eq. (2.16). Such a procedure assumes that the magnetic anisotropy and the molecular axes are the same in the solid state and in solution. This is somewhat unjustified. An example of this procedure is shown in Table 2.10.

If single-crystal EPR data are available, the magnetic susceptibility tensor components can be indirectly estimated for $S = \frac{1}{2}$ systems such as low spin iron(III). The splitting of the d orbitals is parameterized in order to obtain the experimental g values. Then the orbital contribution is evaluated and used to calculate the magnetic susceptibility [67,68,99].

The procedure based on the direct use of the g tensor anisotropy and Eq. (2.19) is quite common for $S = \frac{1}{2}$ systems, since g values from frozen solutions are easily obtainable. In this case, both the second order Zeeman contributions and possibly the effects of temperature on the g values are neglected. Furthermore, the directions of the molecular axes are arbitrarily assumed unless single-crystal data are available. The latter is a most unjustified assumption, since the principal axes of the χ or g

tensors, unless fixed by symmetry, are very dependent on small orbital mixing, thus giving rise to a large range of errors in the determination of the geometrical coordinates.

Other semiquantitative methods for evaluating the metal-centered pseudocontact contributions to the shifts are based on the predicted pattern of the pseudocontact shifts according to the ratios of the geometric factors. Eq. (2.14), which is valid for the axial case, can be rewritten as

$$\delta^{\text{pc}} = G_{r,\theta} \cdot D_\chi \quad (2.30)$$

where $G_{r,\theta}$ is the geometric factor and D_χ is the term containing the magnetic susceptibility. Since the latter term is constant for a given molecule, the ratios between the pseudocontact shifts should be the same as the ratios between the $G_{r,\theta}$ values calculated assuming axial symmetry. When this equation is obeyed, it can be concluded that the observed hyperfine shifts are mainly pseudocontact in origin. In other cases this same property allows the pseudocontact contribution on all nuclei to be estimated by assuming that at a certain nucleus position the contact contribution is negligible. A section will be devoted to this case in paramagnetic metalloproteins. Horrocks has developed a method [49] which is based on a comparison between the proton hyperfine shift pattern for a molecule where the shifts are only contact in origin, and an analogous molecule whose proton shifts have to be factorized.

In the case of high spin iron(III) porphyrins, La Mar et al. [58] factorized the shifts by exploiting the different temperature dependence of contact and pseudocontact shifts. In fact, the observed hyperfine shifts were found to follow a relation of the type

$$\delta^{\text{pc}} = \alpha T^{-1} + \beta T^{-2} \quad (2.31)$$

where the T^{-1} dependence was attributed to the contact term and the T^{-2} dependence to the metal-centered pseudocontact term (see Eqs. (2.5) and (2.29)).

For low spin hemoproteins there are attempts in the literature to determine the magnetic susceptibility anisotropy and principal directions from the hyperfine shifts of the heme methyl carbons and of the attached protons. Neither the crystal structure nor the magnetic properties of the studied hemoprotein are required. The method proposed by Yamamoto et al. [100] is based on McConnell's equation (Eq. (2.25)), according to which the contact shifts of the heme methyl carbons and of the attached protons are directly proportional to the unpaired electron density in the p_z orbital of the pyrrole carbon bearing the methyl group. Therefore, a plot of the contact shifts for the heme methyl carbon resonances vs. the same quantity for the attached proton resonances should be linear and should intercept zero. Deviations from a straight line should arise from differences in the metal-centered pseudocontact contributions experienced by carbons on the one hand and protons on the other [99]. A best fitting procedure is applied to minimize the deviations of the above plot from linearity, by optimizing the $\Delta\chi$ values of Eq. (2.14) and the orientation of the χ -tensor with respect to the heme. The method may be useful to provide a first glance estimate of the

χ -tensor parameters. However, it is now becoming evident that the McConnell proportionality constant varies from methyl to methyl in these low symmetry systems [101].

A second approach is due to Turner [102]. It assumes that the z magnetic axis is perpendicular to the heme mean plane. The hyperfine shifts of the carbon nuclei of the heme methyls are considered only contact in origin because the latter are expected to be much larger than the pseudocontact shifts. From the carbon contact shifts, through the help of simple Hückel MO calculations, the linear combinations of the e_g (d_{xz} , d_{yz}) orbitals are calculated, which describe the ground and excited states in rhombic symmetry like in proteins. Finally the g values and the magnetic anisotropy are calculated and from the latter the pseudocontact shifts. This method is reliable enough if the assumption of the z magnetic axis is valid, which may not always be the case [103].

2.8. The case of lanthanides and actinides

2.8.1. Electronic properties of lanthanides

The electronic properties of lanthanides are peculiar, in that spin–orbit interactions are very large, larger in fact than ligand field effects. Therefore, a somewhat different formalism is used.

Spin–orbit interactions couple the orbital L and spin S angular momenta. The resulting free ion terms are characterized by J values which are vector combinations of L and S . Again the level of interest is the ground level, which is that with largest S , largest L with equally large S , smallest J for f^1 to f^6 lanthanides, and largest J for f^8 to f^{13} lanthanides (Table 2.11). For example, Ce(III) has a ground state with $J = \frac{5}{2}$, since one electron in an f orbital gives rise to a free ion term 2F with $S = \frac{1}{2}$ and $L = 3$. Two terms arise through spin–orbit coupling: one with $J = 3 - \frac{1}{2} = \frac{5}{2}$ and the other with $J = 3 + \frac{1}{2} = \frac{7}{2}$. The former term is the ground state, as shown in Table 2.11. The J values of the ground state vary from $\frac{5}{2}$ to 8, including $J = 0$ for Eu(III) and Sm(II). In general, it can be assumed that the ground term is the only one of interest; however, this is not true for Sm(III), which has an excited J manifold at about 1000 cm^{-1} , and Eu(III), whose ground term has $J = 0$ and would be diamagnetic if excited terms were not taken into consideration.

In actinides, the J terms are closer in energy and more heavily admixed by spin–orbit coupling.

Ligand field effects split the J manifold in a way that is not easily predicted without specific calculations. However, the overall splitting is such that many of the levels are appreciably populated at room temperature. An elegant procedure that takes such effects into account in a general way with respect to pseudocontact shifts of metal-centered origin has been provided by Bleaney [104].

2.8.2. The pseudocontact contribution to the hyperfine shifts

Ligand field effects remove the spherical symmetry around the metal ion and cause magnetic susceptibility anisotropy. The pseudocontact shifts are then given by

Table 2.11
Some electronic properties of lanthanide ions

Ion	Configuration	$^{2S+1}L_J$ of ground state (multiplicity in parentheses)	g_J^a	$\langle S_z \rangle_J^b$	$\langle S_z \rangle_J^c$	δ^{pc} (ppm) ^d
Ce ³⁺	4f ¹	² F _{5/2} (6)	6/7	1.07	0.98	+1.6
Pr ³⁺	4f ²	³ H ₄ (9)	4/5	3.20	2.97	+2.7
Nd ³⁺	4f ³	⁴ I _{9/2} (10)	8/11	4.91	4.49	+1.05
Pm ³⁺	4f ⁴	⁵ I ₄ (9)	3/5	4.80	4.01	−0.6
Sm ³⁺	4f ⁵	⁶ H _{5/2} (6)	2/7	1.79	−0.06	+0.17 ^e
Eu ³⁺ (Sm ²⁺)	4f ⁶	⁷ F ₀ (1)	—	—	−10.68	~ −1.0 ^e
Gd ³⁺ (Eu ²⁺)	4f ⁷	⁸ S _{7/2} (8)	2	−31.5	−31.50	~0
Tb ³⁺	4f ⁸	⁷ F ₆ (13)	3/2	−31.5	−31.82	+20.7
Dy ³⁺	4f ⁹	⁶ H _{15/2} (16)	4/3	−28.30	−28.54	+23.8
Ho ³⁺	4f ¹⁰	⁵ I ₈ (17)	5/4	−22.50	−22.63	+9.4
Er ³⁺	4f ¹¹	⁴ I _{15/2} (16)	6/5	−15.30	−15.37	−7.7
Tm ³⁺	4f ¹²	³ H ₆ (13)	7/6	−8.17	−8.21	−12.7
Yb ³⁺	4f ¹³	² F _{7/2} (8)	8/7	−2.57	−2.59	−5.2

^a Calculated from Eq. (2.32). The equation does not hold for f⁶ ions. ^b Calculated according to Eq. (2.35). ^c Calculated by inclusion of the excited states [105]. ^d Pseudocontact shift predicted from Eq. (2.34) for $r = 300$ pm, $3\cos^2\theta - 1 = 1$, $T = 300$ K, and D_z values for each lanthanide estimated from Ref. [104]. ^e Including contributions from excited J manifolds [104]. For f⁶ ions, the contribution of the ground state manifold is zero.

Eq. (2.16). As already mentioned in Section 2.6 for high spin iron(III), the susceptibility can be factorized into two contributions: one is given by a Zeeman term of the type $g\mu_B B_0 S_z$, and the other is given by the splitting of the magnetic manifold, which provides anisotropy. As the orbital and spin angular momenta are strongly coupled, the g factor in lanthanide free ions is a function of both L and S and of their vector combination J ; it is given by

$$g_J = 1 + \frac{J(J+1) - L(L+1) + S(S+1)}{2J(J+1)} \quad (2.32)$$

and the Zeeman term then becomes $g_J \mu_B B_0 J_z$. Note that when $L=0$, $g_J=2$, and when $S=0$, $g_J=1$, as expected. In analogy with Eq. (2.5), the Zeeman contribution provides a term in T^{-1} . If D is larger than the Zeeman energy and smaller than kT , the term which introduces the ligand field splitting is a term in T^{-2} (see Eq. (2.29)). The general expression is [104]

$$\delta^{pc} = -\frac{\mu_0}{4\pi} \frac{g_J^2 \mu_B^2 J(J+1)(2J-1)(2J+3)}{60(kT)^2} \times \frac{D_z(3\cos^2\theta - 1) + (D_x - D_y)\sin^2\theta \cos 2\Omega}{r^3} \quad (2.33)$$

where r , θ , and Ω are the polar coordinates of the nucleus with respect to the principal directions of the D tensor (Section 1.4), and g_J is given by Eq. (2.32)

(Table 2.11). Eq. (2.33) differs from Eq. (2.29) in that only the term in T^{-2} has remained. In fact, in the present approximation, g_J is isotropic.

For axial symmetry, Eq. (2.33) becomes

$$\delta^{\text{pc}} = -\frac{\mu_0}{4\pi} \frac{g_J^2 \mu_B^2 J(J+1)(2J-1)(2J+3)}{60(kT)^2} \frac{D_z(3\cos^2\theta - 1)}{r^3} \quad (2.34)$$

The parameter D_z accounts for crystal field effects, assuming that the splitting of the $2J+1$ levels does not exceed kT in energy. The shifts at 300 K for a nucleus at 300 pm from the metal and $3\cos^2\theta - 1 = 1$, calculated following Bleaney's treatment [104] and using a plausible value for the ligand field parameter to calculate D_z for each lanthanide, are reported in the last column of Table 2.11 and in Fig. 2.26. For Sm(III), the shift value has been obtained by also considering the first excited $J = \frac{7}{2}$ manifold. For Eu(III), the ground state $J = 0$ does not contribute to the shift; instead, the excited levels with $J = 1$ and $J = 2$, which lie at about 400 and 1200 cm^{-1} above it, provide the pseudocontact shift, which has a rather complex temperature dependence.

For f^7 ions, the ligand field splitting is zero under first-order conditions, whereas higher order effects account for the splitting of the $J = \frac{7}{2}$ level and for a small pseudocontact shift.

The accuracy of the present point-dipole approximation with respect to a model with delocalized unpaired electrons (Section 2.2.2) has also been evaluated for f^n systems [106]. The deviations have been found to be substantially smaller than those estimated for 3d metal ions.

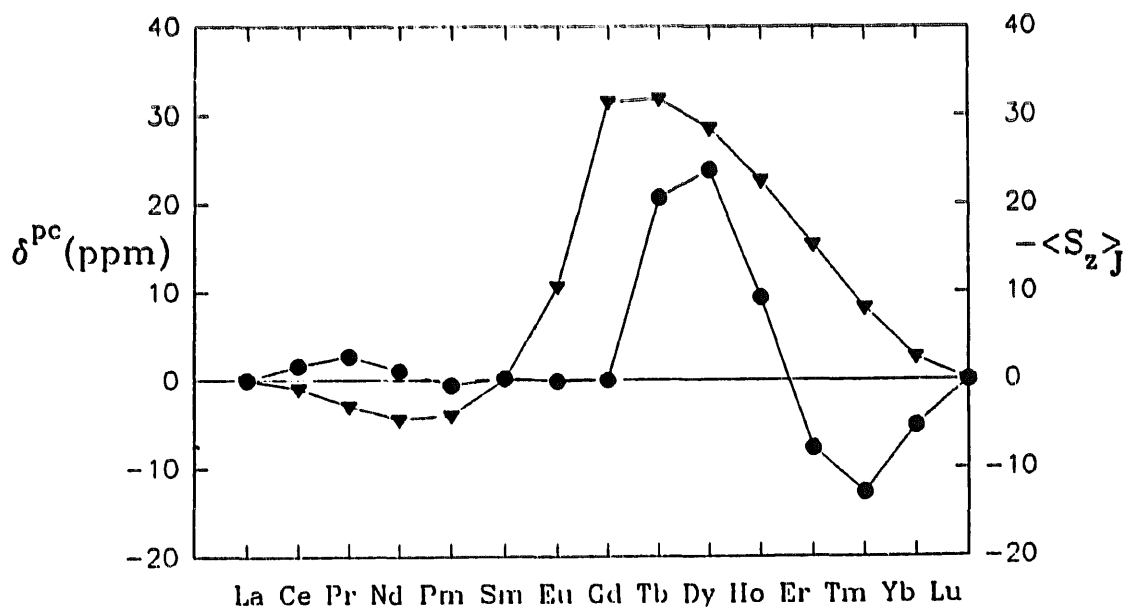


Fig. 2.26. Calculated patterns of: dipolar shifts (●) [104] and $-\langle S_z \rangle_J$ (▼) [105] values (proportional to the contact shifts) induced by lanthanide ions.

2.8.3. The contact contribution to the hyperfine shifts

Although the contact contribution can be sizable and sometimes dominant for ^{17}O and ^{14}N nuclei directly coordinated to the metal [105], it is often negligible for nuclei a few bonds apart from the metal ion, unless efficient spin delocalization mechanisms are operative. The contact shift can be evaluated (see Eq. (2.5)) through the expectation value $\langle S_z \rangle_J$ on the ground J manifold, the Zeeman splitting of which is less than kT [107]:

$$\langle S_z \rangle_J = -g_J(g_J - 1)J(J + 1) \frac{\mu_B B_0}{3kT} \quad (2.35)$$

In this approximation, g_J is isotropic (see, however, Chapter 8). We need to consider $\langle S_z \rangle_J$ and not $\langle J_z \rangle$ because only the spin is delocalized onto the molecule. The evaluation of $\langle S_z \rangle_J$ is made by considering the actual separation of the M_J levels [105]. The contact contribution is therefore

$$\delta^{\text{con}} = \frac{A}{h} \frac{g_J(g_J - 1)\mu_B J(J + 1)}{3\gamma_I kT} \quad (2.36)$$

or

$$\delta^{\text{con}} = \frac{1}{\mu_0} \frac{A}{h} \frac{g_J - 1}{\gamma_I \mu_B g_J} \chi \quad (2.37)$$

Although this simple treatment does not take into account the ligand field splitting of the J manifold, it provides a useful criterion for predicting the general trend of contact shifts along the series. Note that this method does not apply to Sm(III) and Eu(III) salts for the reason already outlined. The values of $\langle S_z \rangle_J$, with or without inclusion of the excited states, are reported in Table 2.11 and in Fig. 2.26. It is noteworthy that $\langle S_z \rangle_J$ in lanthanides can be either negative or positive owing to the large orbital contribution to the determination of the energy levels. Since orbital contributions are larger than spin contributions, $\langle S_z \rangle_J$ can also differ in sign with respect to the spin-only value.

It is also often assumed that A is constant along a series of lanthanide complexes with the same ligand. The mechanism providing spin density delocalization from the metal to the ligands is due to a weak covalent bonding involving the 6s metal orbital, which, in turn, can transfer unpaired spin density on nearby nuclei through spin polarization from 4f orbitals [107].

2.8.4. Separation of pseudocontact and contact contributions

The following method for separation of pseudocontact and contact shifts, proposed by Dobson et al. [108], is valid for axial systems assuming that: (1) there is a nucleus in such a position in the molecule that the contact contribution is zero because it is far from the paramagnetic center; (2) the contact hyperfine coupling is constant ($\pm 10\%$) for Nd–Tm.

For nuclei i and j :

$$\frac{\delta_i^{\text{pc}}}{\delta_j^{\text{pc}}} = R_{ij} \quad (2.38)$$

If $\delta_j^{\text{con}} = 0$, then the ratio of the total hyperfine shifts δ^{hyp} for nuclei i and j is

$$\frac{\delta_i^{\text{hyp}}}{\delta_j^{\text{hyp}}} = R_{ij} + \frac{\delta_i^{\text{con}}}{\delta_j^{\text{iso}}} = R_{ij} + \frac{A}{h} \frac{g_J(g_J - 1)\mu_B J(J + 1)}{3\gamma_N k T \delta_j^{\text{iso}}} \nu_0 \quad (2.39)$$

By plotting $\delta_i^{\text{iso}}/\delta_j^{\text{iso}}$ vs. $g_J(g_J - 1)J(J + 1)/\delta_j^{\text{iso}}$ for all the lanthanides, the intercept gives R_{ij} and hence the ratio between pairs of pseudocontact shifts (Fig. 2.27). The requirement for axial symmetry apparently holds for many systems, even with low symmetry, possibly as a result of ligand rearrangement which might be fast on the NMR time scale.

Separation of pseudocontact and contact shifts in axial systems can also be achieved, again by using a variety of lanthanides, without assuming that for a given signal the contact shift is zero, as long as the patterns of both pseudocontact and contact shifts (Fig. 2.26) hold. Here, the hyperfine shift can be expressed as the sum of contact and pseudocontact shifts (Eqs. (2.36) and (2.34)):

$$\delta_{ij}^{\text{hyp}} = \delta_{ij}^{\text{con}} + \delta_{ij}^{\text{pc}} = K A_i \langle S_z \rangle_j + G_i D_j \quad (2.40)$$

where the subscript i refers to the observed nucleus and j to the lanthanide employed (cf. Eq. (2.30)). $\langle S_z \rangle_j$ and C_j depend only on the lanthanide, whereas A_i and G_i are

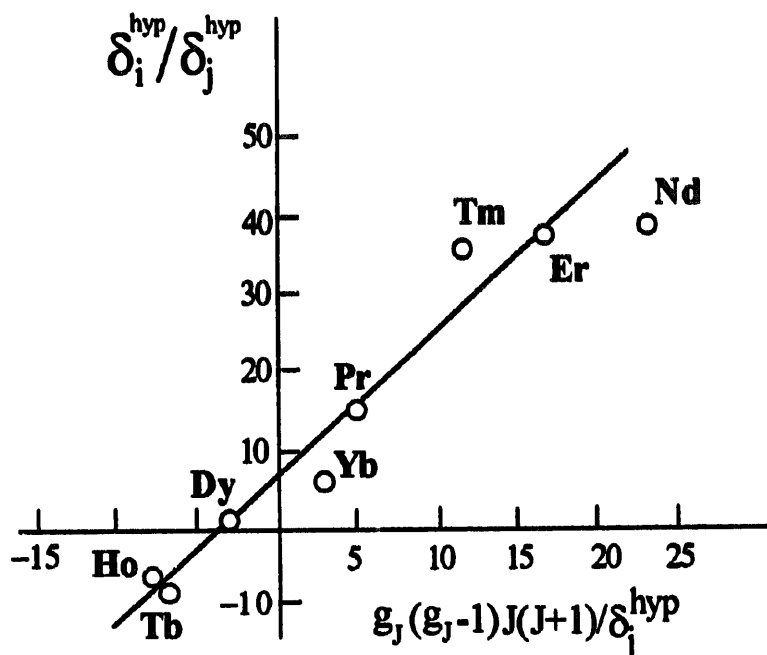


Fig. 2.27. Observed ratios between the hyperfine shifts of the ^{31}P (δ_i^{hyp}) and ^1H (δ_j^{hyp}) resonances of cytidine monophosphate interacting with lanthanide ions, as a function of $g_J(g_J - 1)J(J + 1)/\delta_j^{\text{hyp}}$ for each lanthanide [108].

assumed to depend only on the nucleus and not on the lanthanide. G_i is given by $(3 \cos^2 \theta_i - 1)/r_i^3$ of Eq. (2.34). The unknowns for a single shift are A_i and G_i . If n signals are observed, the unknowns are $2n$; that is, A_i and G_i for the n nuclei. For a second lanthanide derivative, A_i and G_i are the same, and the experimental data are now $2n$ — that is, as many as the unknowns. By using a variety of lanthanides, it is possible, in general, to set up and solve the appropriate number of simultaneous equations and thus evaluate the terms A_i and G_i for each nucleus [109–111]. This procedure is again valid as long as A_i and G_i depend only on the nucleus, and $\langle S_z \rangle_j$ and C_j depend only on the lanthanide in a predictable way and not on the nucleus under observation. The accuracy of the results depends on how precisely the patterns of Fig. 2.26 are capable of reproducing the contact and pseudocontact shifts within the lanthanide series. As we have seen, precise estimates of $\langle S_z \rangle$ in the equation for δ^{con} (Eqs. (2.35) and (2.36)) require evaluation of the splitting of the manifold for the particular complex examined; the equation for δ^{pc} (Eq. (2.34)), besides being valid only for axial symmetry, assumes that the splitting of the $2J + 1$ levels does not exceed kT . It has been pointed out that such an assumption is not correct [112], although a thorough treatment [113] has shown that Eqs. (2.33) and (2.34) are capable of accounting for pseudocontact shifts at or near room temperature with an accuracy of 10–20%.

When contact contributions can be neglected, the pseudocontact shifts for ligand protons in series of lanthanide complexes can be reproduced by using the complete equation for non-axial cases (Eq. (2.33)) and the geometric factors calculated from the X-ray structure [114–120]. The values for the D_z and $D_x - D_y$ parameters obtained through best fitting procedures are in fair to good agreement with the single-crystal anisotropy data [116–120].

2.8.5. Lanthanides as pseudocontact shift reagents

The f^n configurations give rise to several free ion terms that upon spin–orbit coupling give rise, except for f^7 configurations (Gd^{3+} , Eu^{2+}), to several closely spaced energy levels. The multiplicity of the ground levels varies from 6 to 17 (Table 2.11), and is further split by crystal field effects. According to the electronic relaxation mechanisms discussed in Section 3.3, the availability of low-lying excited levels accounts for short electronic relaxation times, again with the exception of metal ions with an f^7 configuration. For these fast-relaxing systems, the correlation times are determined by the electronic relaxation times. Values for the latter have been estimated from nuclear relaxation measurements (see Section 3.4).

Short electronic relaxation times result in very little line broadening, besides Curie relaxation (Section 3.6), of NMR signals. The hyperfine shifts are mainly pseudocontact in origin and the contact contribution, which arises from covalent bonds, is small owing to the strong radial contraction of the f orbitals. The hyperfine coupling constant presumably has a lower value than that of the $3d$ transition metal ions, for the same type of nuclei. Although some ions have been found to give rise to larger contact contributions than other ions of the series, such contributions are generally neglected for nuclei not directly coordinated to the metal. Factorization of the

hyperfine shifts can in principle be successfully achieved by utilizing different lanthanides and assuming that the pseudocontact shifts have axial symmetry (see Section 2.8.4). The combined effects of negligible line broadening and dominant pseudocontact shifts, which depend on the geometrical coordinates described in Eqs. (2.33) and (2.34), justify the use of these ions and their complexes as shift reagents, and they are frequently used in inorganic chemistry. Since these systems have fast electronic relaxation times, the availability of high magnetic fields enables exploitation of Curie relaxation (Section 3.6) for an independent estimate of the distance of the resonating nucleus from line broadening measurements.

The successful use of lanthanides as pseudocontact shift reagents is also due to their tendency to interact with molecules containing oxygen and nitrogen as donor atoms. For example, lanthanide complexes with ligands of the type shown in Fig. 2.28 interact with organic molecules, possibly of biological interest. Pseudocontact shifts (and relaxation measurements) may then allow mapping of the nuclei in the molecule of interest according to the guidelines given in Section 3.12. Progress in this direction is being made. It has been shown that solution structures of lanthanide complexes can indeed be achieved by using pseudocontact shifts and relaxation data together with a structural model as a starting point [121]. By allowing the internal coordinates to change within a relatively narrow range around the average values obtained from

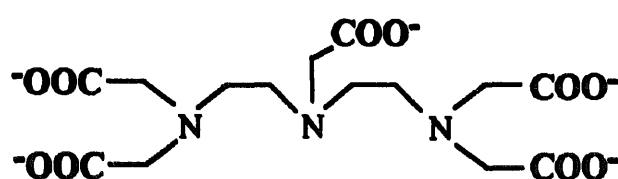
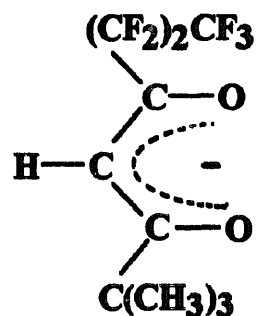
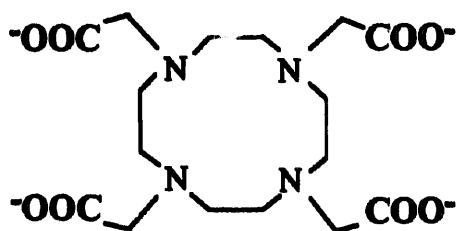
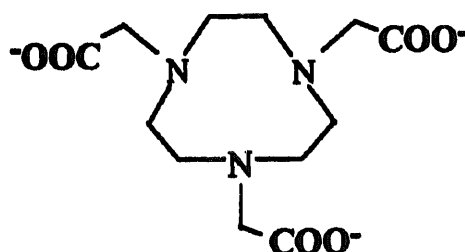
**DTPA****FOD****DOTA****NOTA**

Fig. 2.28. Some lanthanide-chelating ligands used as pseudocontact shift reagents.

crystallographic data, a best fit can be achieved of the experimental pseudocontact shifts. The resulting set of coordinates is then checked against the known constraints imposed by the chemical bonds and bond angles in the complex [121].

2.9. The pseudocontact shifts in paramagnetic metalloproteins

In paramagnetic metalloproteins there are many nuclei close to the paramagnetic center as a result of the folding of the protein chain. Such nuclei, if separated from the metal ion by several chemical bonds, can experience only pseudocontact shifts. We are in the lucky situation of having many of these nuclei, and in principle the many experimental data may provide the polar coordinates of the nuclei within the molecular axes defined by the magnetic anisotropy according to Eq. (2.16). Of course, the signal assignment should be made available independently through COSY and NOESY experiments (see Chapter 8), and the diamagnetic shift should also be known. The latter requirement is rather critical since the diamagnetic shifts extend over a wide range, for instance because of the vicinity of aromatic moieties; therefore, the assignment of a diamagnetic analog should be available.

In practice, the atomic coordinates are needed to extract the five parameters of the equation for the pseudocontact shifts (Eqs. (2.16) or (2.33)). Such parameters are $\Delta\chi_{\parallel}$ (or D_z), $\Delta\chi_{\perp}$ (or $D_z - D_y$), r , θ and Ω in the molecular axis frame: with five pseudocontact shifts and the geometric coordinates of the corresponding nuclei from the X-ray structure, the five parameters can be determined. However, the exact coordinates *in solution* are not available and a number of pseudocontact shifts are needed. Low spin ferric heme containing proteins have been studied [122,123], as well as four- [124] and five-coordinated [125] high spin cobalt(II)-containing proteins. Lanthanides have been used from the early times [126–128], but the problem of the assignment of unpredictably shifted signals was a major one. For these reasons pseudocontact shifts, by themselves, were not deemed suitable for structure determinations.

As we have seen in Section 2.8.5, this view starts being revised [121]. Nowadays, from the spin patterns of COSY or TOCSY spectra (see Chapter 9), it is possible to assign some signals (a minimum of five) and then, iteratively from the calculated magnetic susceptibility tensor, further assignments are achievable which improve the tensor and so on [129]. This opens the way to structural refinements in solution. It has recently been proposed that, given an X-ray structure and a number of pseudocontact shifts of assigned nuclei, refinement of a structure in solution is possible [130]. In other words, the pseudocontact shifts determine the tensor, and then the atomic coordinates are allowed to change in order to best fit the tensor requirements. It is, of course, possible that the refined structure requires a somewhat modified tensor, and that a self-consistent approach is needed.

References

- [1] H.M. McConnell and D.B. Chesnut, J. Chem. Phys., 28 (1958) 107.
- [2] B.R. McGarvey, J. Chem. Phys., 53 (1970) 86.

- [3] G.N. La Mar, J.P. Jesson and P. Meakin, *J. Am. Chem. Soc.*, 93 (1971) 1286.
- [4] H.M. McConnell and R.E. Robertson, *J. Chem. Phys.*, 29 (1958) 1361
- [5] R.M. Golding and L.C. Stubbs, *J. Magn. Reson.*, 33 (1979) 627.
- [6] A.D. Buckingham and P.J. Stiles, *Mol. Phys.*, 24 (1972) 99; P.J. Stiles, *Mol. Phys.*, 27 (1974) 501; P.J. Stiles, *Mol. Phys.*, 29 (1975) 1271.
- [7] R.M. Golding, R.O. Pascual and L.C. Stubbs, *Mol. Phys.*, 31 (1976) 1933.
- [8] J.P. Riley and W.T. Raynes, *Mol. Phys.*, 33 (1977) 619.
- [9] R.M. Golding, R.O. Pascual and J. Vrbancich, *J. Mol. Phys.*, 31 (1976) 731.
- [10] R. Beringer and M.A. Heald, *Phys. Rev.*, 95 (1954) 1474.
- [11] I. Bertini, C. Luchinat and Z. Xia, *Inorg. Chem.*, 31 (1992) 3152.
- [12] A.M. Chmelnick and D. Fiat, *J. Chem. Phys.*, 51 (1969) 4238.
- [13] I. Bertini, C. Luchinat and Z. Xia, *J. Magn. Reson.*, 99 (1992) 235.
- [14] J. Reuben and D. Fiat, *Inorg. Chem.*, 6 (1967) 579.
- [15] N. Bloembergen and L.O. Morgan, *J. Chem. Phys.*, 34 (1961) 842.
- [16] Z. Luz and R.G. Shulman, *J. Chem. Phys.*, 43 (1965) 3750.
- [17] Y. Ducommun, K.E. Newman and A. Merbach, *Inorg. Chem.*, 19 (1980) 3696.
- [18] I. Bertini, F. Briganti, C. Luchinat and Z. Xia, *J. Magn. Reson.*, 101 (1993) 198.
- [19] I. Bertini, F. Capozzi, C. Luchinat and Z. Xia, *J. Phys. Chem.*, 97 (1993) 1134.
- [20] T.J. Swift and R.E. Connick, *J. Chem. Phys.*, 37 (1962) 307.
- [21] Y. Ducommun, W.L. Earl and A.E. Merbach, *Inorg. Chem.*, 18 (1979) 2754.
- [22] W.B. Lewis, M. Alei, Jr. and L.O. Morgan, *J. Chem. Phys.*, 45 (1966) 4003.
- [23] J. Reuben and D. Fiat, *J. Chem. Phys.*, 51 (1969) 4909.
- [24] R.J. Fitzgerald and R.S. Drago, *J. Am. Chem. Soc.*, 89 (1967) 2879.
- [25] J.P. Quaegebeur, C. Chachaty and T. Yasukawa, *Mol. Phys.*, 37 (1979) 409.
- [26] B.B. Wayland, W.L. Rice, *Inorg. Chem.*, 6 (1967) 2270.
- [27] S.K. Sheppard, G.R. Eaton and S.S. Eaton, *Inorg. Chem.*, 28 (1989) 4496.
- [28] J.A. Happe and R.L. Ward, *J. Chem. Phys.*, 39 (1963) 1211.
- [29] R.W. Kluiber and W.DeW. Horrocks, Jr., *Inorg. Chem.*, 6 (1967) 166.
- [30] R.H. Holm, G.W. Everett and W.DeW. Horrocks, Jr., *J. Am. Chem. Soc.*, 88 (1966) 1071.
- [31] G.M. Zhidomirov, P.V. Schastnev and N.D. Chuvylkin, *J. Struct. Chem.*, 11 (1970) 458.
- [32] R.E. Cramer and R.S. Drago, *J. Am. Chem. Soc.*, 92 (1970) 66.
- [33] S. Ito and Y. Yano, *Bull. Chem. Soc. Jpn.*, 57 (1984) 2824.
- [34] K. Hayamizu, M. Murata and O. Yamamoto, *Bull. Chem. Soc. Jpn.*, 48 (1975) 1842.
- [35] D.M. Doddrell and J.D. Roberts, *J. Am. Chem. Soc.*, 92 (1970) 6839.
- [36] I. Bertini, G. Canti, C. Luchinat and F. Mani, *J. Am. Chem. Soc.*, 103 (1981) 7784.
- [37] W.D. Wheeler, S. Kaizaki and J.I. Legg, *Inorg. Chem.*, 21 (1982) 3248.
- [38] F.-J. Wu, D.M. Kurtz, Jr., *J. Am. Chem. Soc.*, 111 (1989) 6563.
- [39] I. Bertini, A. Dikii, C. Luchinat and F. Mani, unpublished results, 1995.
- [40] I. Bertini, D. Gatteschi and A. Scozzafava, *Inorg. Chim. Acta*, 6 (1972) 185.
- [41] I. Bertini, C. Luchinat and A. Scozzafava, *Inorg. Chim. Acta*, 19 (1976) 201.
- [42] G.N. La Mar, W.DeW. Horrocks, Jr. and L.C. Allen, *J. Chem. Phys.*, 41 (1964) 2126.
- [43] I. Bertini, D.L. Johnston and W.DeW. Horrocks, Jr., *Inorg. Chem.*, 9 (1970) 693.
- [44] I. Bertini, C. Luchinat and A. Scozzafava, *Inorg. Nucl. Chem. Lett.*, 15 (1979) 89.
- [45] N.M. Karayannis, C.M. Mikulski and L.L. Pytlewski, *Inorg. Chim. Acta*, 5 (1971) 69.
- [46] R.W. Kluiber and W.DeW. Horrocks, Jr., *J. Am. Chem. Soc.*, 87 (1965) 5350.
- [47] G.N. La Mar and G.R. Van Hecke, *Inorg. Chem.*, 9 (1970) 1546.
- [48] I. Bertini and L.J. Wilson, *J. Chem. Soc. Inorg. Phys. Theor.*, (1971) 489.
- [49] W.DeW. Horrocks, Jr., *Inorg. Chem.*, 9 (1970) 670.
- [50] M.L. Wicholas and R.S. Drago, *J. Am. Chem. Soc.*, 90 (1968) 2196.
- [51] C. Benelli, I. Bertini and D. Gatteschi, *J. Chem. Soc. Dalton Trans.*, (1972) 661.
- [52] D.R. Eaton, A.D. Josey, W.D. Phillips and R.F. Benson, *J. Chem. Phys.*, 37 (1962) 347.
- [53] D.R. Eaton, A.D. Josey, R.E. Benson, W.D. Phillips and T.L. Cairns, *J. Am. Chem. Soc.*, 84 (1962) 4100.

- [54] R.H. Holm and C.J. Hawkins, in G.N. La Mar, W.DeW. Horrocks, Jr. and R.H. Holm (Eds.), *NMR of Paramagnetic Molecules*, Academic Press, New York, 1973, pp. 243–332.
- [55] J.T. Groves, R.C. Haushalter, M. Nakamura, T.E. Nemo and B.J. Evans, *J. Am. Chem. Soc.*, 103 (1981) 2884.
- [56] H. Tsurumaki, Y. Watanabe and I. Morishima, *J. Am. Chem. Soc.*, 115 (1993) 11784.
- [57] G.N. La Mar and F.A. Walker, *J. Am. Chem. Soc.*, 95 (1973) 6950.
- [58] G.N. La Mar, G.R. Eaton, R.H. Holm and F.A. Walker, *J. Am. Chem. Soc.*, 95 (1973) 63.
- [59] M.M. Maltempo, T.H. Moss and M.A. Cusanovich, *Biochim. Biophys. Acta*, 351 (1974) 237.
- [60] A.D. Boersma and H.M. Goff, *Inorg. Chem.*, 21 (1982) 581.
- [61] F.A. Walker and G.N. La Mar, *Ann. N.Y. Acad. Sci.*, 206 (1973) 328.
- [62] D.L. Budd, G.N. La Mar, K.C. Langry, K.M. Smith and R. Nayyir-Mazhir, *J. Am. Chem. Soc.*, 101 (1979) 6091.
- [63] J. Mispelter, M. Momenteau and J.-M. Lhoste, *J. Chem. Soc. Dalton Trans.*, (1981) 1729.
- [64] G.N. La Mar, J.T. Jackson, L.B. Dugad, M.A. Cusanovich and R.G. Bartsch, *J. Biol. Chem.*, 265 (1990) 16173.
- [65] A. Mayer, S. Ogawa, R.G. Shulman, T. Yamane, J.A.S. Cavaleiro, A.M.d'A. Rocha Gonsalves, G.W. Kenner and K.M. Smith, *J. Mol. Biol.*, 86 (1974) 749.
- [66] I. Bertini, F. Capozzi, C. Luchinat and P. Turano, *J. Magn. Reson.*, 95 (1991) 244.
- [67] W.DeW. Horrocks, Jr. and E.S. Greenberg, *Biochim. Biophys. Acta*, 322 (1973) 38.
- [68] J. Trehwella and P.E. Wright, *Biochim. Biophys. Acta*, 625 (1980) 202.
- [69] L.P. Yu, G.N. La Mar and K. Rajarathnam, *J. Am. Chem. Soc.*, 112 (1990) 9527; S.D. Emerson and G.N. La Mar, *Biochemistry*, 29 (1990) 1545.
- [70] D.L. Turner and R.J.P. Williams, *Eur. J. Biochem.*, 211 (1993) 555; N.V. Shokhirev and F.A. Walker, *J. Phys. Chem.*, 99 (1996) 17795.
- [71] G.N. La Mar, D.L. Budd and H.M. Goff, *Biochem. Biophys. Res. Commun.*, 77 (1977) 104.
- [72] H.M. Goff and G.N. La Mar, *J. Am. Chem. Soc.*, 99 (1977) 6599.
- [73] J.D. Satterlee and G.N. La Mar, *J. Am. Chem. Soc.*, 98 (1976) 2804; G.N. La Mar and F.A. Walker, *J. Am. Chem. Soc.*, 95 (1973) 1790.
- [74] L. Banci, I. Bertini, S. Marconi and R. Pierattelli, *Eur. J. Biochem.*, 215 (1993) 431.
- [75] I. Bertini, G. Gori, C. Luchinat and A.J. Vila, *Biochemistry*, 32 (1993) 776.
- [76] H.M. Goff, G.N. La Mar and C.A. Reed, *J. Am. Chem. Soc.*, 99 (1977) 3641; B.R. McGarvey, *Inorg. Chem.*, 27 (1988) 4691.
- [77] I. Bertini, P. Turano and A.J. Vila, *Chem. Rev.*, 93 (1993) 2873.
- [78] E.W. Stone and A.H. Maki, *J. Chem. Phys.*, 37 (1962) 1326.
- [79] M. Karplus, *J. Am. Chem. Soc.*, 85 (1963) 2870.
- [80] M. Karplus and G.K. Fraenkel, *J. Chem. Phys.*, 35 (1961) 1312.
- [81] E.T. Strom, G.R. Underwood and D. Jurkowitz, *Mol. Phys.*, 24 (1972) 901.
- [82] W. Derbshire, *Mol. Phys.*, 5 (1962) 225.
- [83] D.R. Eaton, A.D. Josey, W.D. Phillips and R.E. Benson, *Mol. Phys.*, 5 (1962) 407.
- [84] I. Bertini, F. Capozzi, C. Luchinat, M. Piccioli and A.J. Vila, *J. Am. Chem. Soc.*, 116 (1994) 651.
- [85] H.M. McConnell, *Proc. Natl. Acad. Sci. USA*, 69 (1972) 335.
- [86] H.M. Goff, in A.B.P. Lever and H.B. Gray (Eds.), *Iron Porphyrins*, Addison-Wesley, Reading, MA, 1983, p. 237.
- [87] H.M. Goff, *J. Am. Chem. Soc.*, 99 (1977) 7723.
- [88] I. Morishima, T. Inubushi, S. Neya, S. Ogawa and T. Yonezawa, *Biochem. Biophys. Res. Commun.*, 78 (1977) 739.
- [89] I. Morishima and T. Inubushi, *J. Am. Chem. Soc.*, 100 (1978) 3568.
- [90] D.V. Behere, E. Gonzales-Vergara and H.M. Goff, *Biochem. Biophys. Res. Commun.*, 131 (1985) 607.
- [91] L. Banci, I. Bertini, I.-C. Kuan, M. Tien, P. Turano and A.J. Vila, *Biochemistry*, 32 (1993) 13483.
- [92] H. Pan and B.C. Gerstein, *J. Magn. Reson.*, 92 (1991) 618.
- [93] A.C. McLaughlin, C. Grathwohl and R.E. Richards, *J. Magn. Reson.*, 31 (1978) 283.
- [94] J.-C. Boubel, J.-J. Delpuech and A. Peguy, *J. Chem. Soc. Dalton Trans.*, (1978) 1506.
- [95] C.P. Bhasin, G. Srivastava and R.C. Mehrotra, *Inorg. Chim. Acta*, 128 (1987) 69.

- [96] G. Labauze and J.B. Raynor, *J. Chem. Soc. Dalton Trans.*, (1981) 590.
- [97] W.DeW. Horrocks, Jr. and D.D. Hall, *Inorg. Chem.*, 10 (1971) 2368.
- [98] R.J. Kurland and B.R. McGarvey, *J. Magn. Reson.*, 2 (1970) 286.
- [99] W.DeW. Horrocks, Jr. and E.S. Greenberg, *Inorg. Chem.*, 10 (1971) 2190.
- [100] Y. Yamamoto, N. Nanai and R. Chujo, *J. Chem. Soc. Chem. Commun.*, (1990) 1556.
- [101] L. Banci, I. Bertini, R. Pierattelli and A.J. Vila, *Inorg. Chem.*, 33 (1994) 4338.
- [102] D.L. Turner, *Eur. J. Biochem.*, 227 (1995) 829.
- [103] K. Rajarathnam, G.N. La Mar, M.L. Chiu and S.G. Sligar, *J. Am. Chem. Soc.*, 114 (1992) 9048.
- [104] B. Bleaney, *J. Magn. Reson.*, 8 (1972) 91.
- [105] R.M. Golding and M.P. Halton, *Aust. J. Chem.*, 25 (1972) 2577.
- [106] R.M. Golding, R.O. Pascual and B.R. McGarvey, *J. Magn. Reson.*, 46 (1982) 30.
- [107] W.B. Lewis, J.A. Jackson, J.F. Lemons and H. Taube, *J. Chem. Phys.*, 36 (1962) 694.
- [108] C.M. Dobson, R.J.P. Williams and A.V. Xavier, *J. Chem. Soc. Dalton Trans.*, (1973) 2662.
- [109] C.N. Reilly, B.W. Wood and J.F. Desreux, *Anal. Chem.*, 47 (1975) 2110.
- [110] J. Reuben and G.A. Elgavish, *J. Magn. Reson.*, 39 (1980) 421.
- [111] J.G. Shelling, M.E. Bjorson, R.S. Hodges, A.K. Taneja and B.D. Sykes, *J. Magn. Reson.*, 57 (1984) 99.
- [112] W.DeW. Horrocks, Jr., *J. Magn. Reson.*, 26 (1977) 333.
- [113] B.R. McGarvey, *J. Magn. Reson.*, 33 (1979) 445.
- [114] R.E. Cramer, R. Dubois and C.K. Furuie, *Inorg. Chem.*, 14 (1975) 1005.
- [115] R.E. Cramer, R. Dubois and K. Seff, *J. Am. Chem. Soc.*, 96 (1974) 4125.
- [116] R.E. Cramer and R.B. Maynard, *J. Magn. Reson.*, 31 (1978) 295.
- [117] M.V.R. Stainer and J. Takats, *J. Am. Chem. Soc.*, 105 (1983) 410.
- [118] B.G. Jenkins and R.B. Lauffer, *Inorg. Chem.*, 27 (1988) 4730.
- [119] C.F.G.C. Geraldes, A.D. Sherry and G.E. Kiefer, *J. Magn. Reson.*, 97 (1992) 290.
- [120] J. Lisowski, J.L. Sessler, V. Lynch and T.D. Mody, *J. Am. Chem. Soc.*, 117 (1995) 2273.
- [121] S. Aime, M. Botta and G. Ermondi, *Inorg. Chem.*, 31 (1992) 4291.
- [122] Y. Gao, J. Boyd, G.J. Pielak and R.J.P. Williams, *Biochemistry*, 30 (1991) 1928.
- [123] S.D. Emerson and G.N. La Mar, *Biochemistry*, 29 (1990) 1556.
- [124] I. Bertini, C. Luchinat, M. Piccioli, M. Vicens Oliver and M.S. Viezzoli, *Eur. Biophys. J.*, 20 (1991) 269.
- [125] L. Banci, L.B. Dugad, G.N. La Mar, K.A. Keating, C. Luchinat and R. Pierattelli, *Biophys. J.*, 63 (1992) 530.
- [126] I.D. Campbell, C.M. Dobson, R.J.P. Williams and A.V. Xavier, *Ann. N.Y. Acad. Sci.*, 222 (1973) 163.
- [127] I.D. Campbell, C.M. Dobson and R.J.P. Williams, *Proc. Roy. Soc. London Ser. A*, 345 (1975) 41.
- [128] L. Lee and B.D. Sykes, *Biochemistry*, 22 (1983) 4366.
- [129] F. Capozzi, M.A. Cremonini, C. Luchinat and M. Sola, *Magn. Reson. Chem.*, 31 (1993) S118.
- [130] M. Gochin and H. Roder, *Protein Sci.*, 4 (1995) 296.